Improving the performance of a shell and tube latent heat thermal energy storage through modifications of heat transfer pipes

Ali, Abdullah Masoud; Bagdanavicius, Audrius; Barbour, Edward R.; Pottie, Daniel L.; Garvey, Seamus; Rouse, James; Baniamerian, Zahra

DOI:
10.1016/j.est.2024.112678

Document Version
Publisher's PDF, also known as Version of record

Citation for published version (Harvard):
Ali, AM, Bagdanavicius, A, Barbour, ER, Pottie, DL, Garvey, S, Rouse, J & Baniamerian, Z 2024, 'Improving the performance of a shell and tube latent heat thermal energy storage through modifications of heat transfer pipes: A comprehensive investigation on various configurations', *Journal of Energy Storage*, vol. 96, 112678. https://doi.org/10.1016/j.est.2024.112678

Journal of Energy Storage 96 (2024) 112678

Contents lists available at ScienceDirect

Journal of Energy Storage

journal homepage: www.elsevier.com/locate/est

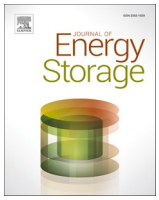

Research Papers

Improving the performance of a shell and tube latent heat thermal energy storage through modifications of heat transfer pipes: A comprehensive investigation on various configurations

Abdullah Masoud Ali [a,*], Audrius Bagdanavicius [a], Edward R. Barbour [b], Daniel L. Pottie [b], Seamus Garvey [c], James Rouse [c], Zahra Baniamerian [c]

[a] School of Engineering, University of Leicester, Leicester LE1 7RH, UK
[b] Centre for Renewable Energy System Technology (CREST), Loughborough University, Loughborough LE11 3TU, UK
[c] Faculty of Engineering, University of Nottingham, Nottingham NG7 2RD, UK

ARTICLE INFO

Keywords:
Latent heat thermal energy storage
Phase change material
Heat transfer pipes
Helical fins
Twisted tape
Modelling

ABSTRACT

The modification of the geometric configurations of heat transfer pipes in shell and tube Latent Heat Thermal Energy Storage (LHTES) systems not only enhances the melting process of the phase change material (PCM) but also improves the overall performance of these systems. This study aims to investigate ways to enhance the performance of LHTES systems by employing heat transfer pipes with various fin and twisted tape arrangements in a horizontal orientation. The Finite Volume Method and Enthalpy-Porosity method are employed to simulate the melting process. Stearic acid is used as the PCM material, while water serves as the heat transfer fluid. Eight different geometric configurations are modelled in the LHTES system: base case, horizontal fins, vertical fins, helical fins, horizontal tape, vertical tape, twisted tape and helical fins with twisted tape. The results show that within the time range of 0 and 29 min, the combined configuration of helical fins with twisted tape consistently demonstrates the fastest melting process. After 29 min, the configuration with vertical fins exhibits a marginally faster melting process than the combined configuration of helical fins with twisted tape. The configurations involving tapes also contribute to accelerated melting, although to a lesser extent than those with fins. Particularly, twisted tape proves highly effective in facilitating faster melting. The complete melting process times for configurations with vertical fins, helical fins, and combined helical fins with twisted tape are 38.7 %, 23.5 % and 32.7 % faster compared to the base case which is ~69 min. Among the configurations, using tapes results in higher flow resistance and surface area compared to the base case. The attractive features of these configurations make them ideal for creating efficient and space-saving energy storage systems. This study provides crucial insights into essential heat and mass transfer processes, which can be leveraged to develop advanced LHTES systems for enhanced performance and sustainable energy solutions.

1. Introduction

The consumption of fossil fuels as the main energy source in various industrial applications has had a significant detrimental impact on the environment, leading to pollution and the release of greenhouse gases [1]. The limitations associated with fossil fuels, such as their non-renewable nature, finite resources, and adverse effects on the environment and climate change, have prompted an increasing motivation to explore different sources of energy that offer reduced carbon intensity and a more environmentally friendly impact [2,3]. However, a big challenge to achieving sustainable energy systems is the balance between the continuous energy supply and demand. To overcome this challenge, the application of effective and reliable thermal energy storage (TES) systems is very important [4]. TES systems play a key part in enabling the reliable production of thermal and reducing energy losses. Furthermore, these systems operate as efficient peak-shaving methods, leading to reduced energy use and environmental pollution [5]. Thermal energy storage systems are also an integral component of thermomechanical energy storage technologies, such as Compressed Air Energy Storage (CAES) systems or Carnot Batteries [6,7].

Among the various thermal energy storage systems, Latent Heat

* Corresponding author.
E-mail address: amsa7@leicester.ac.uk (A.M. Ali).

https://doi.org/10.1016/j.est.2024.112678
Received 24 January 2024; Received in revised form 11 June 2024; Accepted 16 June 2024
Available online 22 June 2024

Nomenclature

Symbols

A	Area m^2
Cp	Specific heat J/kg
D_h	Hydraulic diameter m
f	The quantity predicted
$\vec{g}$	Gravitational acceleration m/s^2
H	Total specific enthalpy J/kg
h	Specific enthalpy J/kg
h_{eff}	Effective heat transfer coeffcient $W/(m^2 \cdot K)$
k	Thermal conductivity W/(m·K)
L	Channel length m
M	Mass kg
Nu	Nusselt number
$\widehat{P}$	The order of convergence
P	twisted tape pitch
p	Pressure Pa
Q	Stored energy J
$\dot{Q}$	Heat transfer rate J/s
Re	Reynolds number
r	The mesh refinement ratio
S	Source term for momentum equation $kg/(m^3 \cdot s)$
T	Temperature K
u	Fluid velocity m/s

Greek symbols

β	Liquid fraction
γ	Thermal expansion coefficient 1/K
Δp	Pressure drop Pa
ε	Relative error
λ	Latent heat of the PCM J/kg
μ	Viscosity kg/(m·s)
ρ	Density kg/m^3

Subscripts

cs	Cross-sectional
f	Fluid
ht	Heat transfer
in	Inlet
ref	Reference
s	Solid

Abbreviations

GCI	Grid Convergence Index
HTF	Heat Transfer Fluid
LHTES	Latent heat thermal energy storage
PCM	Phase change material
TES	Thermal energy storage

Thermal Energy Storage (LHTES) systems occur as a beneficial solution. LHTES use Phase Change Materials (PCMs) with high latent heat capacities to store and release heat. PCMs have several advantages, including a high energy storage density and the capability of using isothermal phase change process [8,9]. Using the thermal properties of PCMs, LHTES systems are used to control fluctuations in Heat Transfer Fluid (HTF) temperature throughout the charging and discharging phases of TES. In the charging phase, the PCMs absorb heat, undergo a phase transformation, and store the thermal energy. On the other hand, in the discharging phase, the PCMs release heat and solidify [10,11].

In spite of the significant advantages of LHTES systems, there are many challenges related to heat transfer efficacy and overall performance. When using PCM, several issues may arise, including prolonged melting and solidification transition times, as well as limited efficiency in heat release and absorption. These problems arise from PCMs because of their low thermal diffusivity and thermal conductivity, as a consequence, the applications of LHTES systems are limited [12,13]. To tackle these challenges, researchers have implemented various methods to improve the LHTES systems. These techniques can be broadly categorized into two main methods. The first method focuses on improving the thermal conductivity of the PCM. Strategies within this category include incorporating nanoparticles into the PCM [14,15], using a variety of PCM materials [16,17], using graphite [18,19], and employing metal porous matrices [20,21]. The second approach involves using encapsulated PCM [22,23], adding fins [24,25], implementing various cylinder-tube geometries [26,27], using helical tubes [28,29] and combining a conical shell with a conical coil [30]. These methods enhance heat transfer, ultimately improving overall efficiency and reducing charging and discharging durations in the LHTES system.

The choice of PCM material significantly affects the heat transfer in LHTES systems, with solid-liquid PCM being the most suitable option among others (solid-solid, solid-liquid, or liquid-gas). Extensive research has been done to investigate various solid-liquid PCM materials, including organic compounds (e.g., paraffin, fatty acids), inorganic compounds (e.g., salt hydrates, metallic), and eutectic mixtures (organic-organic, inorganic-organic, inorganic-inorganic) [31]. The choice of PCM for LHTES systems involves defining system requirements, finding temperature ranges, evaluating thermal properties, considering cycling stability, analysing costs and availability, performing simulations or experiments to evaluate the performance of different PCMs under realistic operating conditions.

Most PCMs used in thermal storage systems have low thermal conductivity. This causes incomplete phase transition, temperature fluctuations and system overheating. To improve the thermal performance, heat transfer surfaces with fins are commonly used within the PCM. The effectiveness of different fin designs have been analysed, including longitudinal fins investigated by Rathod and Banerjee [32], circular fins studied by Jung and Boo [33], plate fins examined by Campos-Celador, et al. [34], and pin fins investigated by Tay, et al. [35]. Longitudinal fin configurations offer simplicity, ease of fabrication, and cost-effectiveness, while circular-finned tubes show superior performance compared to pinned tubes in various shell-and-tube configurations. Additionally, the number and location of fins are also principal considerations that would be considered to increase heat transfer between the PCM and HTF in LHTES systems [31]. The ideal choice of tubes and fin materials also plays an important part in achieving optimal thermal performance in the LHTES system. The performance of several metal materials has been examined, such as copper as studied by *Al*-Abidi et al. [36], aluminium as examined by Baby and Balaji [37] and steel as examined by Choi and Kim [38]. When tubes and fin material with lower thermal conductivity cannot achieve the proper heat transfer between the PCM and HTF in the LHTES system, higher thermal conductivity material serves as an effective alternative. Table 1 shows key outcomes from the latest investigations on several fin designs in LHTES systems.

Extensive studies have been carried out to discover how to enhance the heat transfer in heat exchangers, via the incorporation of swirl flow generators. These swirl flow generators have proven to be useful in enhancing flow mixing while generating an acceptable pressure drop, as a result, the heat transfer is enhanced. The twisted tape configurations have been approved as a commonly adopted solution in heat exchangers [39]. When the fluid flows in a tube with a twisted tape, it gains a rotational motion from the twisted tape. This swirl motion then interrupts the thermal boundary layer near the inner tube wall, resulting in strong flow mixing. Therefore, the enhanced heat transfer exceeds

Table 1
Key findings in recent studies on fin designs in LHTES systems using PCM.

Investigated by	Method	Design	Main finding
Mehta, et al. [46]	LHTES Experimental Stearic acid	Helical fin	Heat transfer is more effective in the middle and lower axial regions for vertical and inclined orientations, whereas the horizontal orientation experiences improved heat transfer in the lower radial region. Inserting fins in the horizontal LHSU reduces melting time by up to 34.1 %.
Zhang, et al. [47]	LHTES Numerical RT35	Helical fins (2 and 4 fins)	Two helical fins show the best thermal performance in vertical LHTES, while four helical finned LHTES achieve optimal performance in horizontal thermal energy storage units. Opposite HTF inlet direction to gravitational acceleration improves thermal performance and ensures a uniform temperature field.
Duan, et al. [24]	LHTES Numerical RT82	Helical fins (4,8 and 16 fins)	The phase change process is enhanced by increasing the fin number from 4 to 16 and by increasing the helical cycle from 1/4 to 1.
Li, et al. [25]	LHTES Numerical Paraffin wax	Helical fins (2, 3 and 4 fins)	Two fins exhibit 30.5 % enhancement in melting compared to base case, while three fins case performs worst with 10.7 % improvement. Penetrating fin into HTF tube slightly enhances melting by 2 % compared to triple fin case in the vertical tube.

Table 2
Studies on the application of twisted tapes in different heat transfer systems.

Investigated by	Method	Design	Main finding
Ali, et al. [41]	Microchannel heat sink Numerical	Twisted tape radial gap	The presence of a twisted tape in the microchannel reduces thermal resistance and bottom temperature by inducing swirl flow. Inserting a straight tape reduces the temperature in comparison to having no tape, but not as much as when using a twisted tape.
Ali, et al. [42]	Microchannel heat sink Numerical	Twisted tape Radial gap Pitch distances	The thermal and hydraulic performance of the heat sink improves by closing the radial gap between the tape and the inner wall. This improvement is achieved through enhanced thermal conduction and the elimination of hydraulic losses resulting from the tape tip gap. A pitch distance of L/4 increases the thermal performance in contrast to the pitch distances of L/2.
Arasteh, et al. [43]	Tube Numerical	Twisted tape Pitch distances	The Nusselt number and friction factor show little change when reducing the pitch distance from L/2 to L/6.
Kurnia, et al. [44]	Helical tube heat exchanger Numerical	Twisted tape	Using a twisted tape in the helical tube induces secondary flow, resulting in enhanced heat transfer. Using a twisted tape in the helical tube is well-suited for water applications with higher Reynolds numbers and lower twisting ratios.

those performed with no twisted tape [40]. Several studies into the performance of twisted tapes have been performed in different applications. For example, the application of twisted tapes was explored in the context of a microchannel heat sink, as revealed in the study carried out by Ali et al. [41,42]. Additionally, the efficacy of twisted tapes was examined in tube configurations, as explored by Arasteh et al. [43]. Numerical investigations by Kurnia et al. [44] focused on the utilisation of twisted tapes in helical tubes. Furthermore, the application of twisted tapes in a double-pipe heat exchanger was investigated by Arjmandi et al. [45]. These studies collectively contribute to understanding the performance characteristics and potential benefits associated with the incorporation of twisted tapes in various heat transfer systems. Table 2 presents several studies investigating the application of twisted tapes in different heat transfer systems.

By employing these improvement techniques, researchers aim to overcome challenges associated with different heat transfer systems. The fundamental principles underlying the enhancement of heat transfer in LHTES systems depend on extending the contact area between the PCM and the heat transfer fluid, enhancing convective heat transfer through improved fluid flow characteristics, and reducing thermal resistance at the PCM-pipe interface. The use of different fin designs in the LHTES systems and the integration of swirl flow generators into the pipelines have proven highly effective in improving heat transfer efficiency and overall system performance. However, despite significant progress in this field, a comprehensive investigation directly comparing the performance of helical fin designs and twisted tape pipe inserts in LHTES systems remains elusive. Therefore, the main goal of this research is to investigate this research gap by carrying out numerical analysis and comprehensive comparison of fins and twisted tape approaches in LHTES systems during the charging process.

This study aims to provide useful knowledge and contribute to the development of LHTES systems. In addition, this study provides a complementary contribution to the field of energy storage by studying the effects of straight fins and tape in both vertical and horizontal orientations in the LHTES. Stearic acid was employed as the PCM, and water served as the heat transfer fluid at a constant Reynolds number of around 10,000 for cases without tape and around 8000 for cases with internal tape to ensure similar inlet velocity. The inlet water flow remained constant at a temperature of 358.15 K, with an initial temperature of 303.15 K. One of the objectives was to observe the impact of buoyancy on the selected configurations and their overall performance in LHTES systems.

2. Methodology

2.1. Mathematical formulation

In this study, a comprehensive numerical analysis based on the enthalpy-porosity model [48], which is used to simulate the melting and solidification of the PCM in a shell and tube LHTES systems in a horizontal orientation, was conducted. The investigated system consists of an inner tube serving as a conduit for the hot water flow, referred to as the Heat Transfer Fluid (HTF). Fig. 1 shows the isometric view of the LHTES and eight different geometric configurations. The fluid and solid domains are discretized, and the heat transfer between them is captured using the conjugate heat transfer approach. The governing equation for heat conduction in a solid is typically described by the heat conduction Eq. (1) [49]:

$$\rho_s \, Cp_s \frac{\partial T_s}{\partial t} = k_s \nabla^2 T_s \tag{1}$$

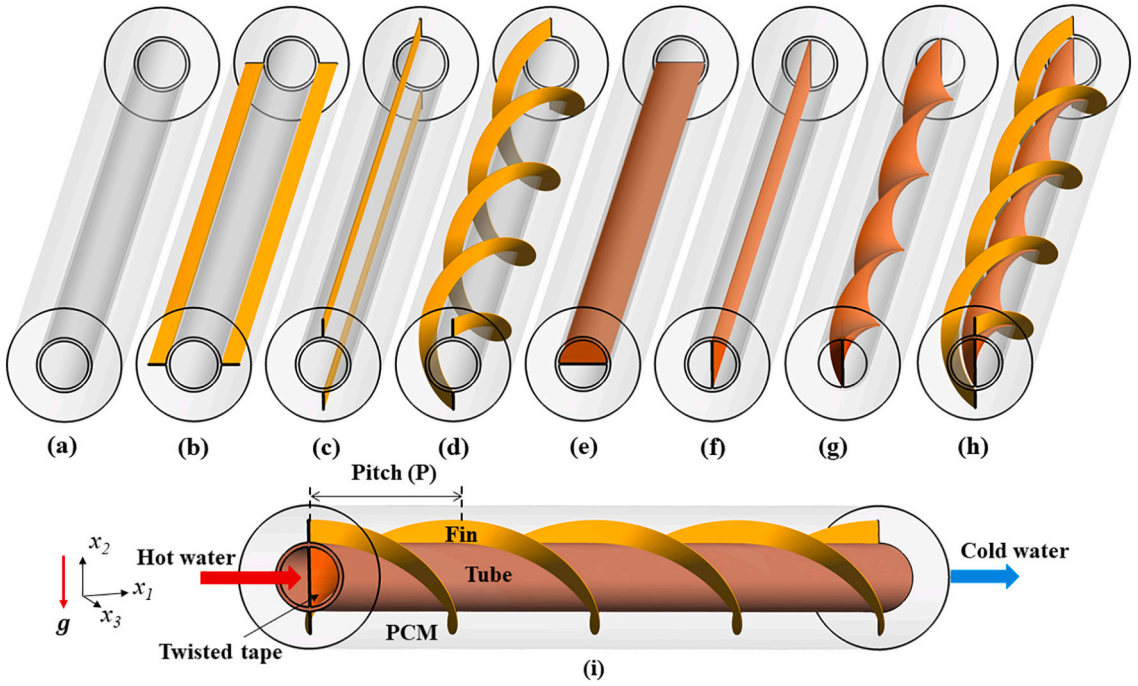

Fig. 1. (a) Base case, (b) horizontal fins, (c) vertical fins, (d) helical fins, (e) horizontal tape, (f) vertical tape, (g) twisted tape, (h) helical fins with twisted tape, (i) isometric view of the LHTES.

Here ρ is density, Cp is heat capacity, k is thermal conductivity and T is temperature.

The Laplace equation is coupled using the time-averaged Navier-Stokes equations that describe the behaviour of the HTF [41]. The numerical solution involves solving the continuity, momentum and energy equations of the HTF, subject to certain assumptions:

1. The flow is three-dimensional and turbulent with temperature dependence and uniform flow velocity at the inlet and Newtonian fluid.
2. The PCM density is assumed constant, and volume change during phase change is neglected. The convection-induced inertia resulting from the density variation due to the temperature difference is considered through a source term added to the momentum equation using the Boussinesq approximation [25].
3. The outer shell wall is insulated, and no heat transfer occurs between the PCM enclosure and the environment.

The HTF governing equations are [28]:

$$\nabla\cdot\left(\rho_{pcm}\,\vec{u}_{HTF}\right)=0 \tag{2}$$

$$\rho_{HTF}\frac{\partial\vec{u}_{HTF}}{\partial t}+\rho_{HTF}\left(\vec{u}_{HTF}\cdot\nabla\right)\vec{u}_{HTF}=-\nabla p_{HTF}+\nabla\cdot\left[(\mu_{HTF}+\mu_t)\nabla\vec{u}_{HTF}\right]+\rho_{HTF}\,\vec{g} \tag{3}$$

$$\rho_{HTF}\,Cp_{HTF}\frac{\partial T_{HTF}}{\partial t}+\rho_{HTF}\left(\vec{u}_{HTF}\cdot\nabla\right)T_{HTF}=\nabla\cdot[(k_{HTF}+k_t)\nabla T_{HTF}] \tag{4}$$

The variables used to describe the properties and boundaries of the working fluid include density ρ, viscosity μ, thermal conductivity k, velocity vector $\vec{u}$, absolute pressure p, absolute temperature T and gravitational acceleration in the ngative x_2 direction $\vec{g}$. Here x_2 represents the axial direction as illustrated in Fig. 1. To consider the turbulent behaviour of the HTF within the inner copper tube, the k-ε turbulence model with Enhanced Wall Treatment is employed to simulate the fluid flow and heat transfer [50]:

$$\frac{\partial}{\partial t}(\rho_{HTF}k_{HTF})+\frac{\partial}{\partial_{r_j}}\left(\rho_{HTF}k_{HTF}\,\vec{u}_j\right)=\frac{\partial}{\partial_{r_j}}\left[\left(\mu_{HTF}+\frac{\mu_t}{\sigma_k}\right)\frac{\partial k_{HTF}}{\partial_{r_j}}\right]+\mu_t\frac{\partial\vec{u}_i}{\partial_{r_i}}\left(\frac{\partial\vec{u}_i}{\partial_{r_j}}+\frac{\partial\vec{u}_j}{\partial_{r_j}}\right)-\rho_{HTF}\varepsilon \tag{5}$$

$$\frac{\partial}{\partial t}(\rho_{HTF}\varepsilon)+\frac{\partial}{\partial_{r_j}}\left(\rho_{HTF}\varepsilon\,\vec{u}_j\right)=\frac{\partial}{\partial_{r_j}}\left[\left(\mu_{HTF}+\frac{\mu_t}{\sigma_\varepsilon}\right)\frac{\partial\varepsilon}{\partial_{r_j}}\right]-\rho_{HTF}C_2\frac{\varepsilon^2}{k_{HTF}+\sqrt{\vartheta\varepsilon}} \tag{6}$$

In the equations above, k and ε represent the turbulence kinetic energy and dissipation rate correspondingly. The turbulent viscosity, μ_t, is defined as $\rho_{HTF}Cp_{HTF}k^2/\varepsilon$. Additionally, the turbulent Prandtl number is denoted as σ. The empirical constants have the following specific values: $\sigma_k=1.0$, $\sigma_\varepsilon=1.3$, and $C_2=1.92$.

The governing equations for the PCM differ from those of the HTF, because of the addition of a source term to the momentum equation using the Boussinesq approximation, and the occurrence of phase transition phenomena. The PCM governing equations are [28]:

$$\nabla\cdot\left(\rho_{pcm}\,\vec{u}_{pcm}\right)=0 \tag{7}$$

$$\rho_{pcm}\frac{\partial\,\vec{u}_{pcm}}{\partial t}+\rho_{pcm}\left(\vec{u}_{pcm}\cdot\nabla\right)\vec{u}_{pcm}=-\nabla p_{pcm}+\mu_{pcm}\nabla^2\vec{u}_{pcm}+\rho_{pcm}\,\vec{g}\,\gamma_{pcm}\left(T_{pcm}-T_{ref}\right)+\mathrm{S} \tag{8}$$

$$\rho_{pcm}\frac{\partial H_{pcm}}{\partial t}+\rho_{pcm}\nabla\cdot\left(\vec{u}_{pcm}H_{pcm}\right)=\nabla\cdot(k_{pcm}\nabla T_{pcm}) \tag{9}$$

The term S is introduced in the momentum equations to account for the influence of phase change on convection [51]:

$$S=\frac{(1-\beta)^2}{(\beta^3-\varepsilon)}\,A_{mush} \tag{10}$$

The term S includes the following parameters: β is the liquid volume fraction, ε is a constant (0.001) that is introduced to avoid division by 0, and A_{mush} is the mushy zone constant. The mushy zone refers to the transitional interface between the fully solid and liquid regions, characterized by a variable volume fraction of cells ranging between 0 and 1 [51].

The total specific enthalpy H is calculated by:

$$H = h + \Delta H \tag{11}$$

where the specific enthalpy h is

$$h = h_{ref} + \int_{T_{ref}}^{T} C_{p,pcm} dT \tag{12}$$

Here: h_{ref} - reference enthalpy, T_{ref} - reference temperature, and C_p - specific heat at a constant pressure. The enthalpy change due to the phase change ΔH is calculated:

$$\Delta H = \beta \lambda \tag{13}$$

where λ and β are the specific latent heat and the liquid fraction of the PCM, respectively. The liquid fraction βcan be described as:

$$\beta = \begin{cases} 0 \text{ if } T < T_s \\ \dfrac{T - T_f}{T_f - T_s} \text{ if } T_s < T < T_f \\ 1 \text{ if } T > T_f \end{cases} \tag{14}$$

where T_f and T_s respectively indicate the liquidus and solidus temperatures of the PCM.

2.2. Geometry and boundary conditions

Fig. 1 illustrates the schematic representation of a shell and tube LHTES. The LHTES system includes a centrally positioned copper tube with a length of 1000 mm. This tube serves as a conduit for the hot water and has an internal diameter D_h of 21 mm and a thickness of 1.5 mm. Additionally, two copper fins are attached to the outer surface of the central tube, each with a radial length of 8 mm and a thickness of 0.5 mm. These fins are symmetrically distributed with equal spacing at intervals of 180°. A pitch distance, P = L/4, is used for the helical fins and twisted tape. The PCM vessel used in this study has an inner diameter of 24 mm and an outer diameter of 50 mm. The geometric dimensions of the LHTES are presented in Table 3. Various configurations of fins and tapes are utilised within the LHTES, as illustrated in Fig. 1(a-h) including: (a) simple pipe – base case, (b) pipe with horizontal fins, (c) pipe with vertical fins, (d) pipe with helical fins, (e) pipe with horizontal tape, (f) pipe with vertical tape, (g) pipe with twisted tape, (h) pipe with helical fins and twisted tape. All pipes, fins and tapes in the LHTES are made from copper to improve the heat transfer between the PCM and the fluid. Table 4 shows the data used for LHTES configurations. The properties of PCM, copper and water are shown in Table 5. In this study, a Reynolds number of around 10,000 was assumed for all cases except those with inner tape, where the Reynolds number was around 8000, to maintain an inlet velocity within the range of 0.45–0.65 m/s. *Re* number characterizes the flow conditions and it is determined based on the inlet conditions using Eq. (15) [52,53]. The flow rate of HTF for configurations without tape was 0.165 kg/s and for configurations with tape was 0.214 kg/s.

Table 3
Geometric dimensions of the pipes in LHTES, in mm.

Inner copper tube diameter	Outer copper tube diameter	Outer diameter	Fin height	Fin and twisted tape width	LHTES length
21	24	50	8	0.5	1000

$$Re = \frac{\rho . u_{in} . D_h}{\mu} \tag{15}$$

Here: ρ is density, u_{in} – velocity, D_h - hydraulic diameter, μ is viscosity.

$$D_h = \frac{4A_{cs}}{P} = \frac{4\left(\frac{\pi}{4}D^2 - ab\right)}{\pi D - 2a + 2b} = \frac{(\pi D^2 - 4ab)}{\pi D - 2a + 2b} \tag{16}$$

Here: A_{cs} is the cross-sectional area, P is the perimeter, and a and b refer to the tape's thickness and width, respectively. In the absence of a tape, the hydraulic diameter D_h is equivalent to D.

In this study, only the melting processes of the PCM are investigated. The outlet of the water tube is subjected to a pressure outlet boundary condition. The inlet flow temperature was set to 358.15 K, while the initial temperature of the PCM was set to 303.15 K, indicating a fully solid state at the start of the simulation.

2.3. Data analysis

The calculation of stored energy Q during the charging process of a PCM can be performed using Eq. (17) [57]:

$$Q = M_{pcm}\left[C_{p,pcm}\left(T_{pcm} - T_{Initial}\right) + \Delta H\right] \tag{17}$$

In this equation $T_{Initial}$ is the initial temperature of the PCM, T_{pcm} is the average temperature of the PCM, $C_{p,pcm}$ is the specific heat capacity of the PCM and M_{pcm} is the mass of the PCM. In the presence of straight fin configurations, the mass of the PCM is lower compared to the base case. Additionally, this mass decreases further when helical fins are implemented.

Nusselt number is calculated using this equation:

$$Nu = \frac{hD_h}{k} \tag{18}$$

Here h is heat transfer coefficient, D_h is hydraulic diameter and k is the thermal conductivity of HTF.

Heat transfer coefficient is found using:

$$h_{eff} = \frac{\dot{Q}}{A_{ht}\left(T_{HTF} - T_{PCM}\right)} \tag{19}$$

Here $\dot{Q}$ is heat transfer rate, A_{ht} is heat transfer area, T_{HTF} is the average temperature of the HTF and T_{PCM} is the average temperature of the PCM.

The pressure drop Δp of the HTF in the pipe between the inlet and outlet can be determined using Eq. (20):

$$\Delta p = p_{in} - p_{out} \tag{20}$$

Here, p_{in} and p_{out} represent the pressure at the inlet and outlet of the HTF tube, respectively..

2.4. Numerical solver

The present study aimed to solve the three-dimensional melting problem numerically using the ANSYS FLUENT software package, version 19.5. The simulation involves multiple steps, starting with geometry creation using Design Modeler, followed by mesh generation in ANSYS Meshing, and then proceeding to CFD simulation and analysis using FLUENT. Finally, the outcomes are processed via ANSYS CFD-Post and Tecplot 360. ANSYS Fluent is a powerful tool for solving fluid flow problems involving solidification and melting. It employs an enthalpy porosity formulation to handle the liquid-solid interface and treats the mushy zone as a porous region with porosity corresponding to the liquid fraction. To account for the pressure drop caused by the solid material, momentum sink terms are included [51]. In this study, the mushy zone parameter was set to a constant value, and the default value of 10^{-5} was chosen [25]. The solution method used to evaluate the pressure-velocity

Table 4
Other LHTES data.

	Base case	Horizontal fins	Vertical fins	Helical fins	Horizontal tape	Vertical tape	Twisted tape	Helical fins with twisted tape
Mass of PCM (kg)	1.736	1.727	1.727	1.726	1.736	1.736	1.736	1.726
Volume of PCM (m^3)	1.510e-3	1.502e-3	1.502e-3	1.501e-3	1.510e-3	1.510e-3	1.510e-3	1.501e-3
Heat transfer area (m^2)	0.075	0.107	0.107	0.146	0.075	0.075	0.075	0.146
Mass flow rate of HTF (kg/s)	0.165	0.165	0.165	0.165	0.214	0.214	0.214	0.214

Table 5
The thermal properties of stearic acid [54], copper [55] and water [56].

	Stearic Acid	Copper	Water
Density ρ (kg/m^3)	1150	8798	998.2
Specific heat C_P (J/kg·K)	2830	381	4182
Thermal conductivity k (W/m·K)	0.29	387.6	0.613
Kinematic viscosity μ ($N{\cdot}s/m^2$)	0.0078	–	0.001003
Thermal expansion coefficient γ (1/K)	0.0008	–	–
Latent heat of fusion λ (J/kg)	186,500	–	–
Solidus temperature (K) T_f	327	–	–
Liquidus temperature (K) T_s	337	–	–

coupling was the SIMPLE method. The HTF flow was analysed using the Standard k-epsilon turbulence model with Enhanced Wall Treatment option [58]. The second-order upwind method was employed to discretize the momentum and energy equations [41]. The pressure correction scheme was set to PRESTO [59] and the gravity (g) options was used. The boundary conditions were defined as follows: the inlet velocity was uniform normal velocity u_{in}, the inlet temperature of HTF was uniform $T_{in} = 358.13$ K. A uniform gauge pressure was set to zero at the outlet. The front, back and the outer shell surfaces were modelled as adiabatic. Interfaces were meticulously established between the outer HTF tube surface and the PCM, and between the HTF and the inner tube surface. The interior walls of the fluid region were set to "no-slip walls" with 'Coupled' thermal conditions. The computations were performed using under-relaxation factors of 0.3, 1, 1, 0.7, 0.9, and 1 for pressure, density, forces, momentum, liquid fraction update, and energy, respectively [58]. The convergence criterion for the continuity, momentum, and energy equations was set to a residual of 10^{-6} [60]. The computational cost of each simulation was 1152 core hours on a 3.2 GHz shared memory high-performance computer cluster.

2.5. Grid independence, time step and Grid Convergence Index (GCI)

This investigation focuses on the accuracy of predictions to 3-D discretization in the computational domains, specifically concerning the average temperature of the PCM in the LHTES with helical fins. To enhance accuracy and reduce simulation time, a hexahedral mesh is preferred over tetrahedral or mixed element meshes [60]. The structured butterfly topology is employed, as it is suitable for hexahedral meshes in pipes. Ansys Design Modeler is utilised for geometric model generation, while Ansys Meshing is employed for creating the structured mesh. Fig. 2(a) and (b) illustrates the average liquid fraction and the predicted average PCM temperature for the helical fins case, respectively, using three grids with different densities (coarse, medium, and fine). Each finer mesh doubles the mesh density. Remarkably, the average liquid fraction and the average PCM temperature display no significant changes with more than 3,041,280 elements. Additionally, Fig. 2(c) shows the average PCM temperature using time steps of 0.8 s, 0.4 s, and 0.2 s for helical fins case. The PCM temperature is still similar at 0.4 s and 0.2 s, leading to the choice of 0.2 s. To further evaluate the impact of spatial discretization on predictions, the Grid Convergence Index (GCI) as per Roache [61], is employed. The order of convergence $\widehat{P}$ is subsequently calculated using Eq. (21):

$$\widehat{P} = ln\left(\frac{(f_3 - f_2)}{(f_2 - f_1)}\right) \tag{21}$$

where f_1 f_2 and f_3 are the quantity predicted for fine, medium and coarse mesh of the average temperature of the PCM in the LHTES with helical fins, at 40 min intervals. To assess the prediction accuracy, the relative error (ε) is calculated between the two finest grids using Eq. (22):

$$\varepsilon_{2,1} = \left|\frac{f_2 - f_1}{f_1}\right| \tag{22}$$

Furthermore, the Grid Convergence Index ($GCI_{2,1}$) is found between these two meshes through Eq. (23):

$$GCI_{2,1} = \frac{f_s|\varepsilon_{2,1}|}{\left(r_{2,1}^{\widehat{P}} - 1\right)} \tag{23}$$

The safety factor (f_s) is 1.25, as utilizing more than two meshes [61]. The mesh refinement ratio (r) is denoted as $r = 2$ reflecting that each successive finer mesh effectively doubles the mesh density. A suitable spatial discretization ensures numerical predictions fall within the asymptotic range of convergence, as represented by Eq. (24):

$$\frac{GCI_{2,1}}{r_{1=2,1}^{\widehat{P}}\, GCI_{3,2}} \cong 1 \tag{24}$$

Examination of Table 6 confirms that the predictions obtained from Eqs. (22) and (23) fall within the asymptotic range of convergence for the finite volume scheme, closely aligning with Eq. (24) as it is close to 1. Considering the GCI analysis in conjunction with examinations from Fig. 2, the mesh of 3,041,280 elements is chosen. Fig. 3 depicts the mesh topology for two of the meshes utilised in the study.

2.6. Validation

In order to determine the accuracy of the numerical predictions, the current numerical model is validated against an experimental study by Khan and Khan [54] and Mahdi, et al. [58]. Fig. 4(a) shows the average PCM temperature during the melting process obtained from an experimental study conducted by Khan and Khan [54]. In this experimental study a shell and tube LHTES with three fins filled with stearic acid was employed as the phase change material. Fig. 4(a) shows an acceptable agreement between the current model and the experimental study.

Fig. 4(b) shows the PCM temperatures at different locations are compared with those obtained from an experimental study by Mahdi, et al. [58]. The numerical predictions of PCM temperatures at points A1, A2, and A3 were utilised in their research to track the evolution of PCM temperature during the melting process at various locations along LHTES. In the experimental investigation conducted by Mahdi, et al. [58], a shell and tube LHTES filled with paraffin wax was employed as the phase change material. Fig. 4 demonstrates a good agreement between the predicted temperatures at A1, A2, and A3 from our numerical model and the temperatures reported by Mahdi, et al. [58] throughout the time range of 0 to 105 min. The maximum deviations between the numerical results and the experimental data were determined to be 0.8 % for point A1, 1.2 % for point A2, and 1.3 % for point A3, respectively. These findings significantly bolster the confidence in the current method utilised for estimating the thermal parameters of the LHTES system.

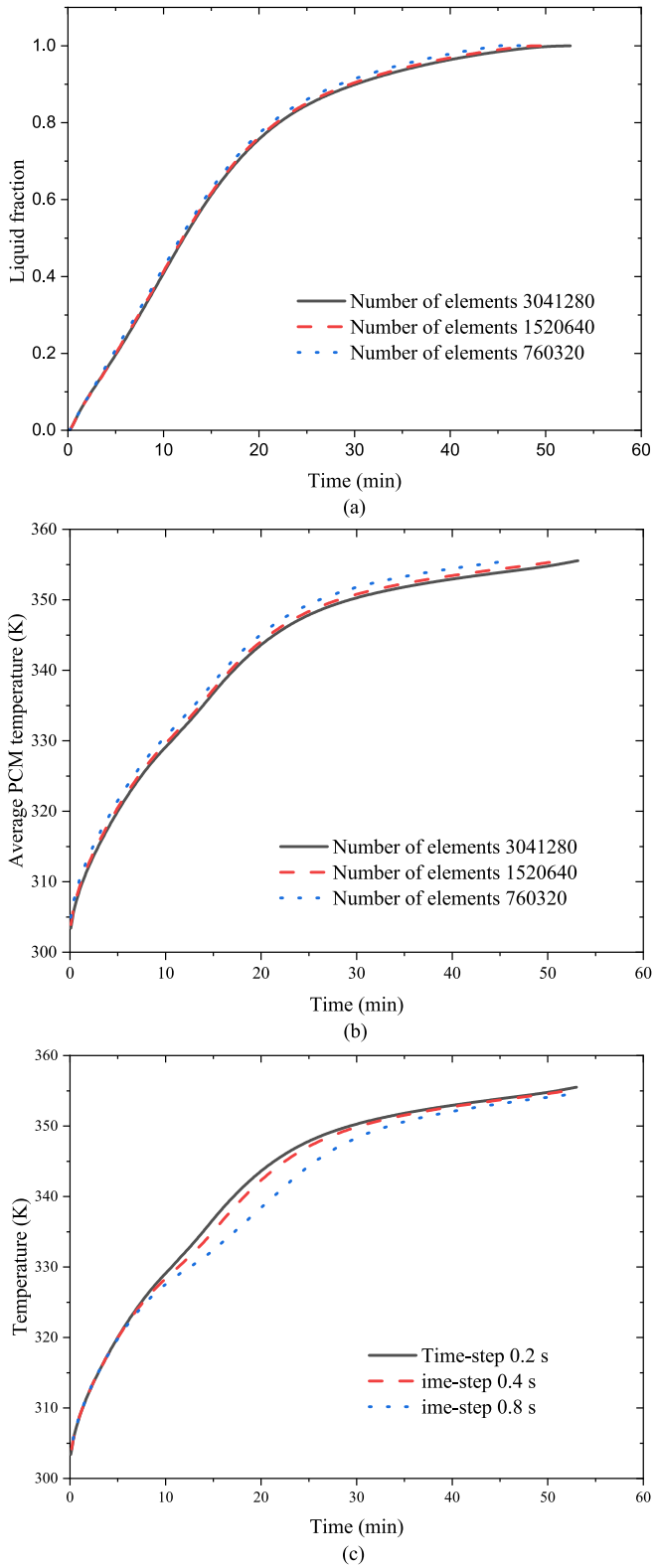

Fig. 2. Grid independence test results of (a) liquid fraction, (b) average PCM temperature, and (c) the time step test of helical fins case.

3. Results and discussion

In this study, eight designs of HTF pipes with various fin and tape configurations have been investigated. This section presents the analysis results of the thermal and hydraulic performance of LHTES systems during the melting process.

Table 6
Mesh convergence parameters on the average PCM temperature of helical fins case, at 20 and 40 min intervals.

Time (min)	Number of elements	$\widehat{p}$	ε	GCI	$\frac{GCI_{3,2}}{\left(r_{2,1}^{\widehat{p}} GCI_{2,1}\right)}$
20	760,320	1	0.0028	0.00334	0.9971
	1,520,640		0.0014	0.00174	
	3,041,280				
40	760,320	1.0057	0.0028	0.00336	0.9971
	1,520,640		0.0014	0.00168	
	3,041,280				

3.1. Effect of fins and tapes on liquid fraction

Fig. 5(a) and (b) displays the visualization of the liquid fraction distribution at four cross-sections in the x_1 plane (the HTF inlet is at the bottom), captured after 5 min from the start. The liquid surface is illustrated using colour isolevels, with red indicating a value of 1, while the solid surface is represented by colour isolevels, where blue corresponds to a value of 0. Fig. 5(a) presents the liquid fraction for the base case, as well as for cases with horizontal fins, vertical fins, and helical fins. The results show that in all instances, the PCM undergoes melting, transforms into a liquid and rises, driven by the thermal convection currents. Similar results have been observed by Mahdi et al. [58]. Notably, the use of horizontal fins, vertical fins, and helical fins increases the liquid fraction significantly. The melting process occurs at a faster rate compared to the base case, and the reasons for this improvement will be further discussed (see Fig. 9). While Fig. 5(a) illustrates a higher liquid fraction using horizontal fins, vertical fins, and helical fins compared to the base case, it remains unclear how the liquid fraction differs among these three configurations.

Fig. 5(b) demonstrates the distribution of liquid fraction for configurations with horizontal tape, vertical tape, twisted tape, and a combination of helical fins with twisted tape. The results show that the use of straight tape in horizontal and vertical orientations leads to a higher liquid fraction compared to the base case at the same time intervals. Furthermore, it is predicted that incorporating a twisted tape in the LHTES configuration will lead to a further increase in the liquid fraction compared to using a straight tape. Also, the combination of helical fins with twisted tape in the LHTES results in the fastest melting process among all cases at 5-min intervals.

Fig. 6 displays the distribution of the liquid fraction in the cross-sectional plane at the midpoint of the LHTES system. The liquid fraction data is presented at 10, 20, 30, and 40-min intervals. Each row represents a different configuration, while the columns correspond to different time instances. The liquid surface is visualized using colour isolevels, where red indicates a value of 1, while the solid surface is depicted by colour isolevels in blue, representing a value of 0. The results demonstrate that the inclusion of fins and tapes leads to a higher liquid fraction than the base case at the same time intervals. This improvement can be attributed to the expanded solid surface area of the HTF tube. Specifically, the configuration with helical fins exhibits a higher liquid fraction than both the horizontal fins and vertical fins configurations in the short time durations, as observed at 10 and 20-min intervals. However, in longer durations, such as 30 and 40 min, the configuration with vertical fins demonstrates a better liquid fraction compared to both helical and horizontal fins, as shown in Fig. 8. Moreover, the inclusion of a twisted tape results in an increased liquid fraction compared to using straight tapes across all time durations. Additionally, the combination of helical fins with twisted tape consistently exhibits the fastest melting process among all cases at 10, 20, and 30-min intervals. However, it is important to note that at 40-min intervals, the vertical fins case shows a slightly faster melting process

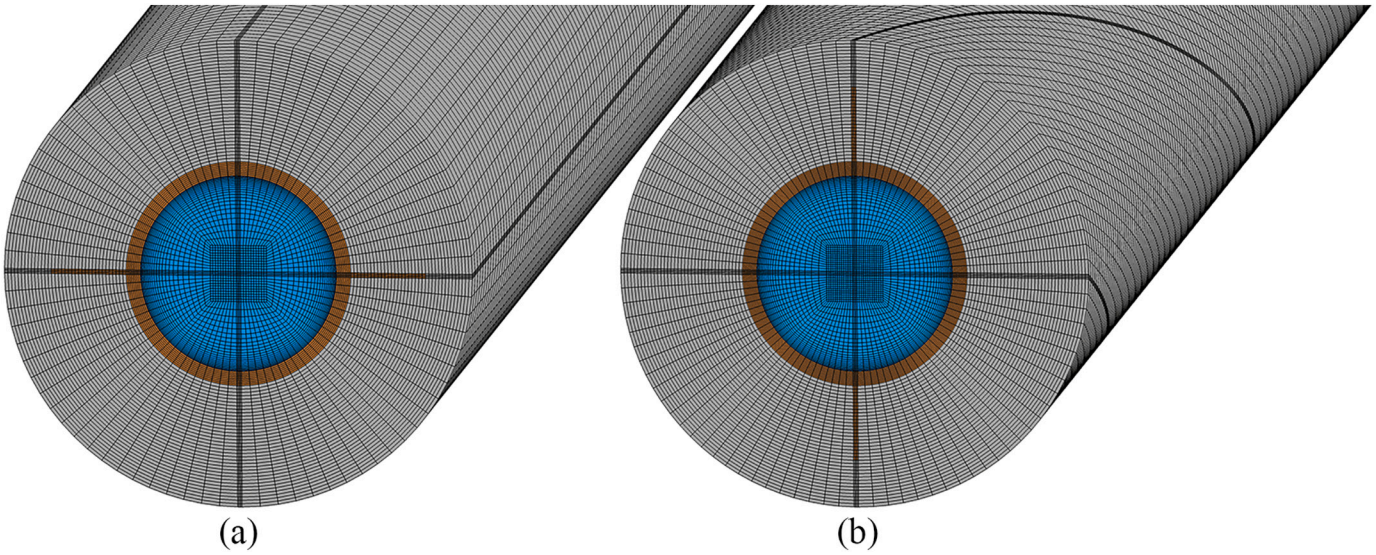

Fig. 3. Three-dimensional mesh structure of (a) horizontal fins configuration and (b) helical fins configuration.

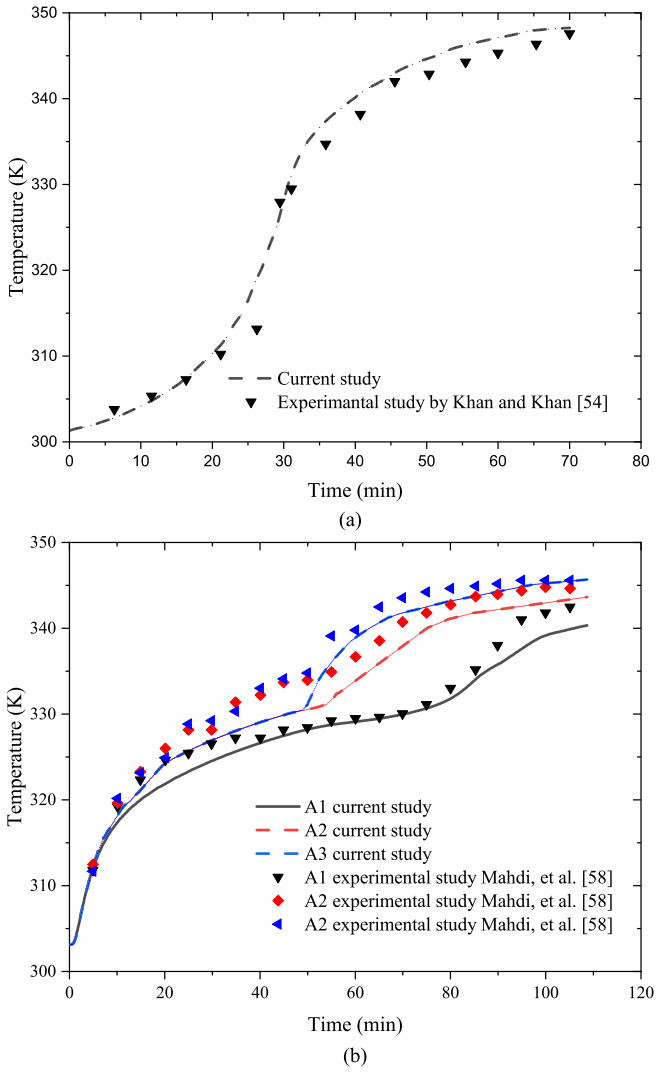

Fig. 4. Validation of numerical results of (a) the average PCM temperature during the melting process conducted by Khan and Khan [54] and (b) the PCM temperatures under the melting process at points A1, A2, and A3 against experimental results conducted by Mahdi et al. [58].

compared to the helical fins with twisted tape configuration.

Fig. 7 shows the convection currents of the liquid phase of PCM in the cross-sectional plane at the midpoint (at a location 500 mm from the inlet) of the LHTES system during a melting process for the base case, helical fins, twisted tape, and helical fins with twisted tape configurations. The data is presented at 10 and 20 min intervals. The results demonstrate that the velocity of the liquid PCM generates a swirling motion within the PCM above the HTF tube. The highest velocity of liquid PCM is observed after 10 min for the base case compared to all other configurations. The addition of fins and tape leads to reduced velocity above the HTF tube. However, due to the addition of fins, the flow of liquid PCM is generated at these fins, thus enhancing energy storage effectiveness and the performance of LHTES.

Fig. 8 displays the distribution of the liquid fraction in the cross-sectional in the x_3 plane of the LHTES system. The liquid fraction data is presented at 40-min intervals. The results demonstrate that the inclusion of vertical fins leads to a higher liquid fraction compared to the other cases at the same time intervals. The primary reason for this improvement is that the lower fin in the vertical configuration is positioned closer to the lower region of the LHTES, helping faster heat-up of the lower region. Moreover, the combination of helical fins with twisted tape exhibits a higher liquid fraction compared to both individual helical fins and twisted tape cases. This improvement can be attributed to the expanded external and internal solid surface of the HTF tube.

Fig. 9 presents the time evolution of the average liquid fraction for various configurations during the melting process in the LHTES system. The configurations include the base case, horizontal fins, vertical fins, helical fins, horizontal tape, vertical tape, twisted tape, and the combined helical fins with twisted tape. The addition of fins and tapes leads to a faster melting process compared to the base case. This improved performance is attributed to the increased surface area of the HTF tube, leading to enhanced convection heat transfer by generating higher thermal convection currents within the PCM, as shown in Fig. 7. The fastest melting process is observed in the time intervals from 0 to 29 min for the combined helical edges with twisted tape configuration. This improved performance is attributed to the increased internal and external surface area of the HTF tube, leading to enhanced heat transfer efficiency. However, it is worth noting that after 29 min, the melting process is slightly faster in the case of the vertical fins compared to the combined configuration of helical fins with twisted tape. Additionally, the results show that the liquid fraction also increases using vertical fins and helical fins configurations compared to the base case at the same time intervals. Particularly, the design with helical fins displays a higher

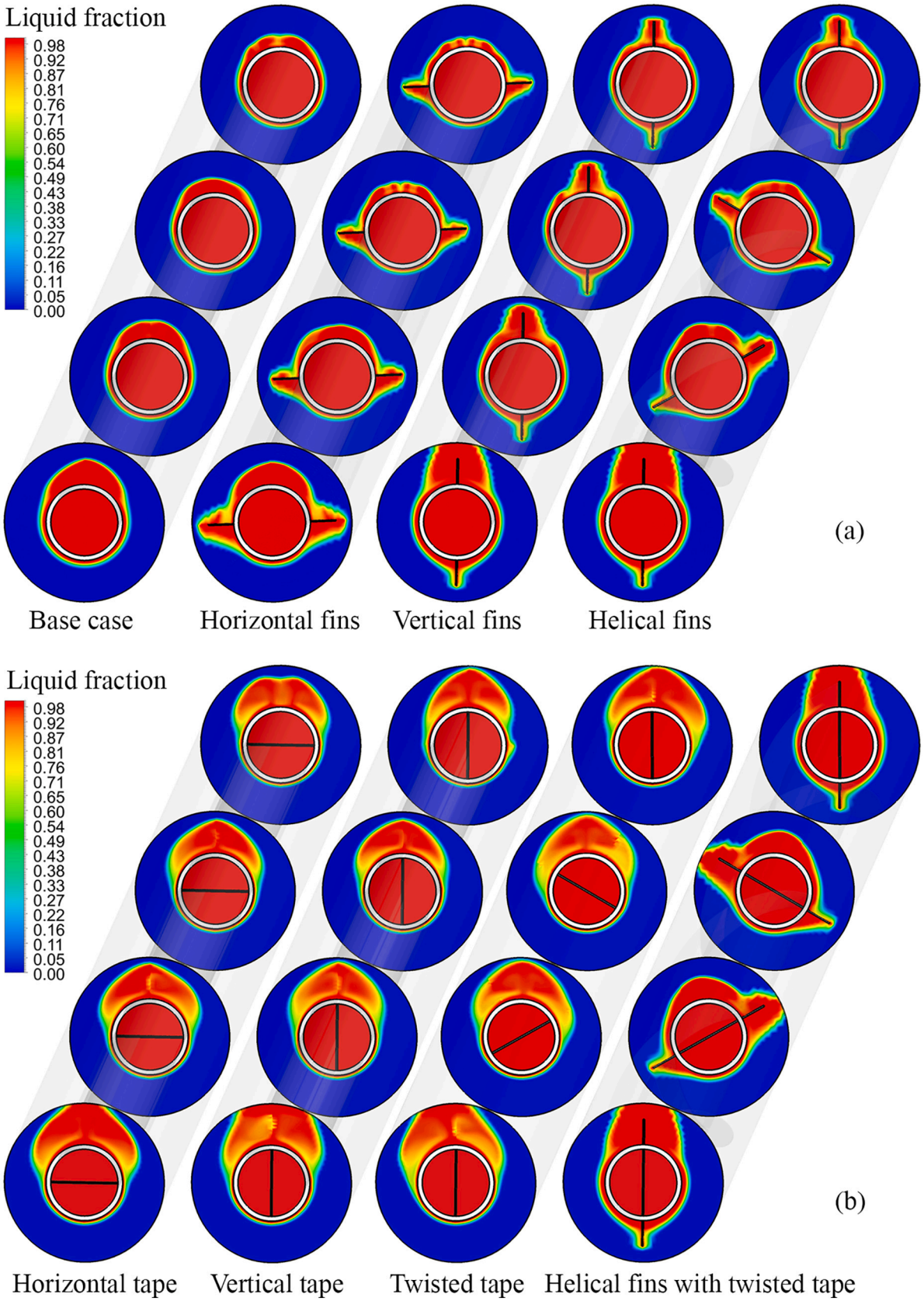

Fig. 5. Liquid fraction during the charging process at four cross-sections in $x_1 = 0, 0.33$ m, 0.66 m and 1 m plane, including (a) the base case, horizontal fins, vertical fins, and helical fins and (b) horizontal tape, vertical tape, twisted tape, and combined helical fins with twisted tape, captured after 5 min from the start. (HTF inlet is the bottom).

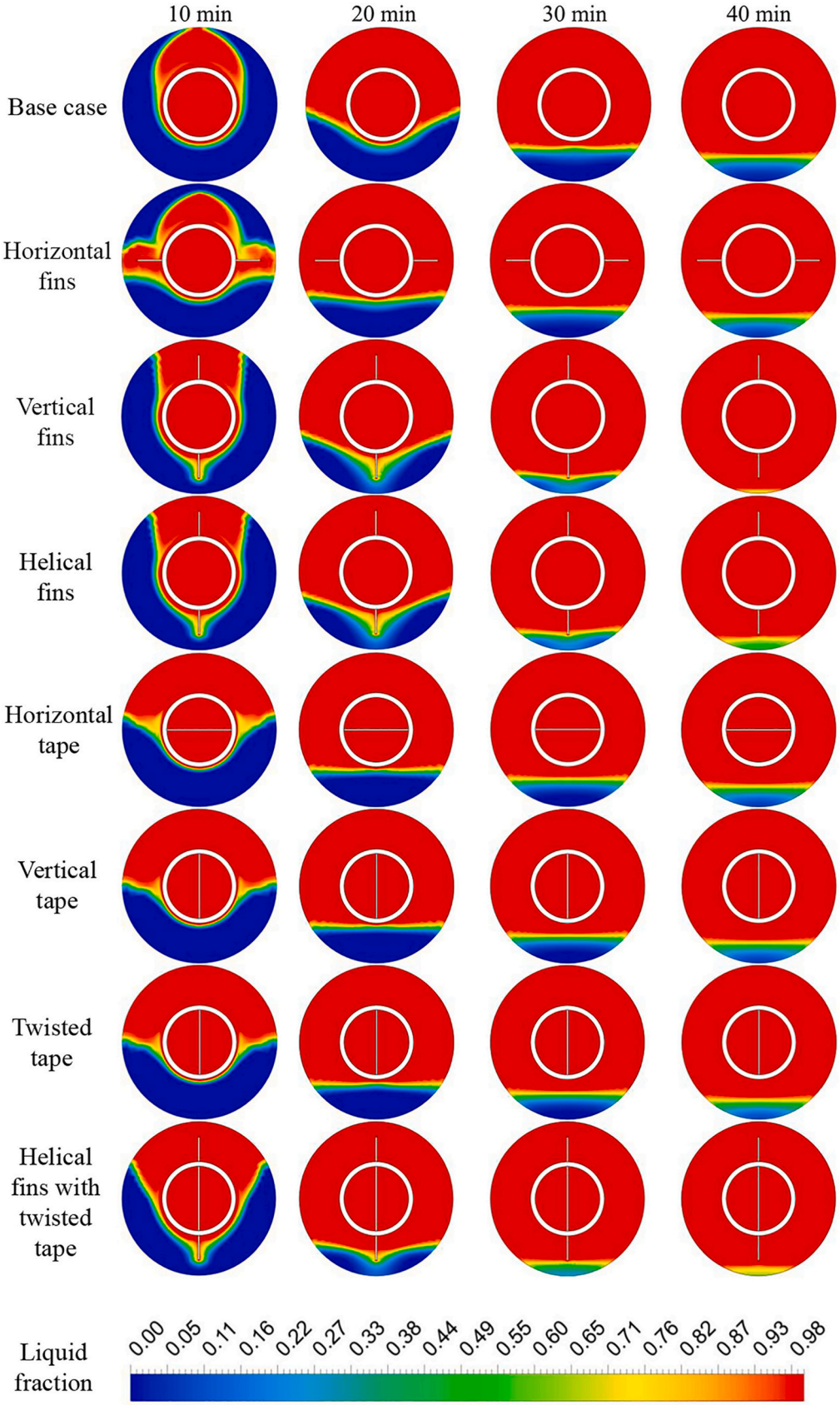

Fig. 6. Liquid fraction of the base case, horizontal fins, vertical fins, helical fins, horizontal tape, vertical tape, twisted tape, and combined helical fins with twisted tape are depicted using colour isolevels at 10, 20, 30, and 40-min intervals. These distributions are shown in the x_1 plane, specifically at a location 500 mm from the inlet.

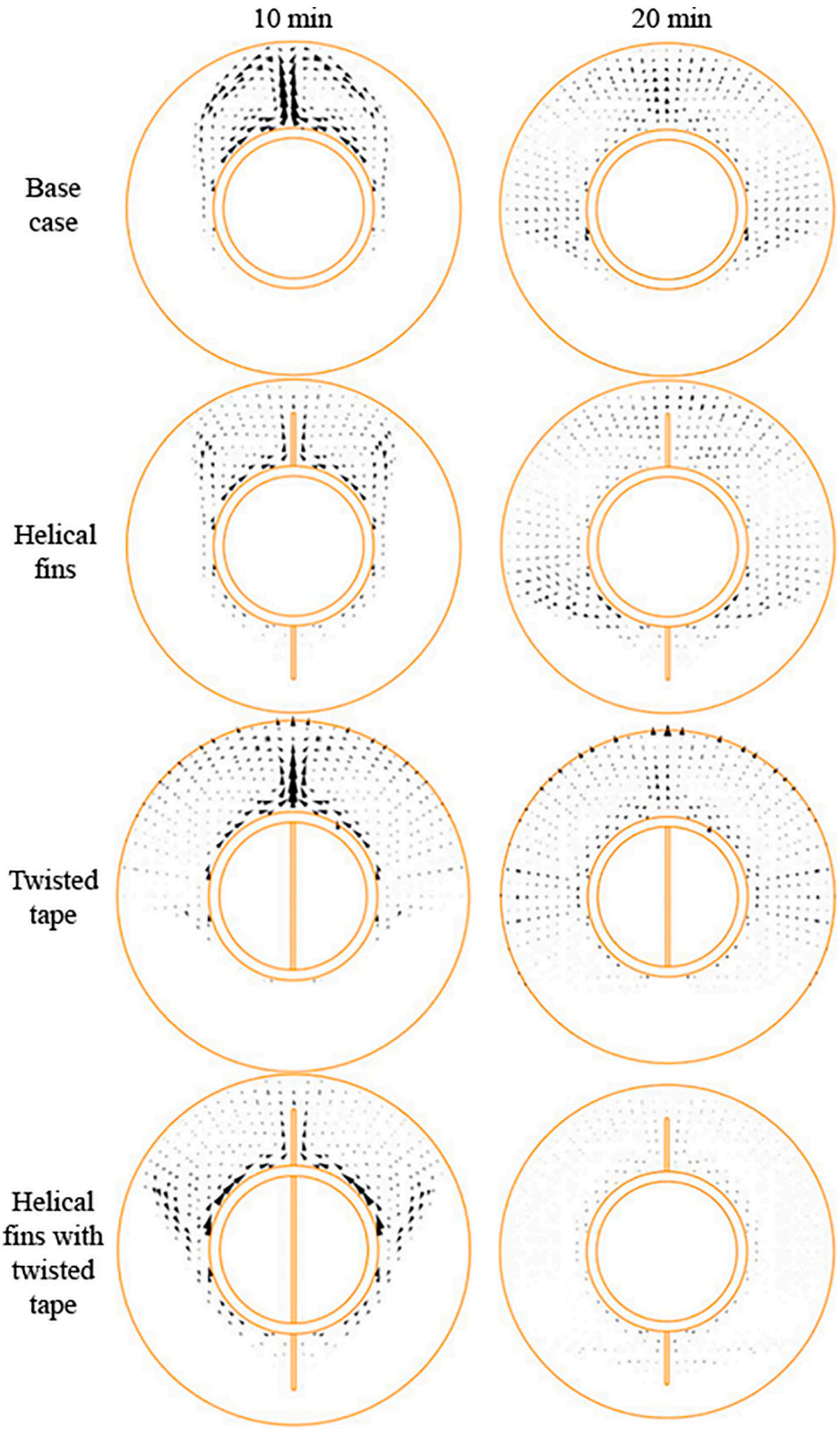

Fig. 7. Velocity vectors of liquid PCM during melting process for the base case, helical fins, twisted tape, and combined helical fins with twisted tape configurations at 10-min intervals, in the x_1 plane, at a location of 500 mm from the inlet.

liquid fraction in comparison to both horizontal and vertical fins within short time durations, as monitored at intervals between 0 and 22 min. This difference is mainly due to the larger surface area of helical fins compared to straight fins, allowing for better contact with the PCM and more efficient heat transfer during the phase change processes. However, in longer durations, the vertical fins demonstrate better heat transfer that leads to a faster increase in liquid fraction compared to both helical and horizontal fins configurations. The placement of the lower fin in the vertical configuration, positioned closer to the lower region of the LHTES, facilitates a faster heat-up of the lower region compared to

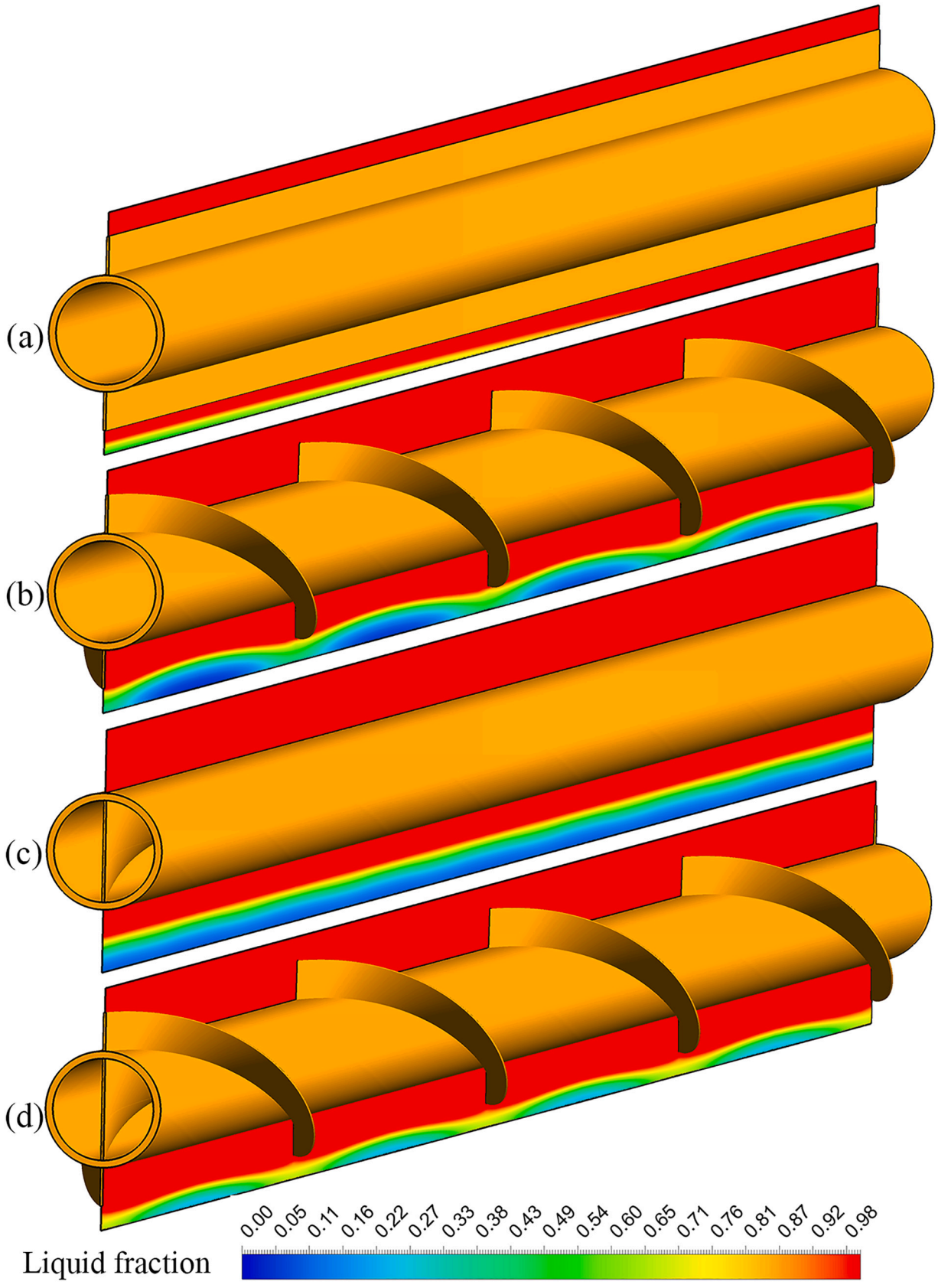

Fig. 8. Liquid fraction of (a) vertical fins, (b) helical fins, (c) twisted tape, and (d) combined helical fins with twisted tape are depicted using colour isolevels at 40-min intervals. These distributions are shown in the x_3 plane.

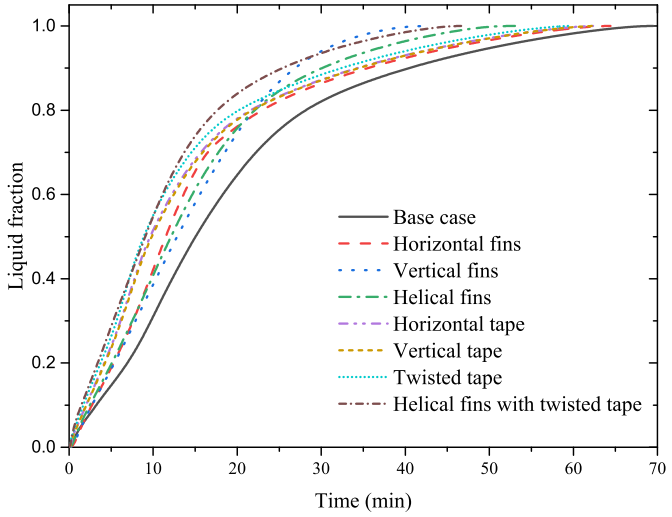

Fig. 9. Liquid fraction evolution over time for the base case, horizontal fins, vertical fins, helical fins, horizontal tape, vertical tape, twisted tape, and combined helical fins with twisted tape, during the melting process.

the configurations with helical and horizontal fins, as illustrated in Fig. 8. The horizontal fins configuration shows a significantly longer full melting process time compared to both the vertical and helical fins, as well as all internal tape configurations. This observation highlights the crucial role that the position of the fins plays in the overall melting process. Moreover, the use of tape also accelerates the melting process, albeit to a lesser extent than fins. The utilisation of straight tape in both horizontal and vertical orientations enhances the development of the liquid fraction compared to the equivalent base case. However, the employment of twisted tape proves more effective in accelerating the melting process. This improved performance is attributed to two key processes: the rotation of the HTF about the central axis, which enhances heat convection currents, introducing an azimuthal velocity component and a higher velocity magnitude as it approaches the wall. Although this rotational flow leads to an increase in pressure drop in the pipe, as shown in Fig. 15, it also induces secondary flow motion in the x_1 plane aiding in the transfer of heat from the HTF to the tube wall. More detailed insights into the heat and mass transfer mechanisms in various twisted tape configurations, including straight and twisted tape, can be found in an extensive research study by Ali, et al. [42]. The complete melting process times for various configurations, including vertical fins, combined helical fins with twisted tape, helical fins, twisted tape, horizontal tape, vertical tape, and horizontal fins, are 38.7 %, 32.7 %, 23.5 %, 14 %, 10.3 %, 10.3 %, and 7.2 % faster than the base case which is ~69 min, respectively. These findings emphasize the significance of appropriate design choices to optimise heat transfer efficiency and accelerate PCM melting, which are crucial considerations for enhancing the performance of latent heat thermal energy storage systems.

3.2. *Effect of fins and tapes on temperature distribution*

Fig. 10 displays the temperature distributions at four cross-sections in the x_1 plane, captured after 5 min from the start. The colour isolevels represent temperature, with red indicating 358.15 K and blue indicating 303.15 K. In Fig. 10(a) the temperature distributions for the base case, and configurations with horizontal fins, vertical fins, and helical fins are shown. The results indicate a consistent temperature decrease of the PCM from the inlet to the outlet for all designs, with the highest temperature observed above the HTF tube at the inlet due to buoyancy effects. The configurations with horizontal fins, vertical fins, and helical fins exhibit higher PCM temperatures compared to the base case. This indicates faster heat transfer from the HTF to the PCM, resulting in a higher temperature. Using the helical fins configuration the highest temperature rise is observed compared to the configurations with vertical and horizontal fins, resulting in more effective heating of the PCM. Fig. 10(b) illustrates the temperature distributions for configurations involving horizontal tape, vertical tape, twisted tape, and a combination of helical fins with twisted tape. The results indicate that using straight tape in horizontal and vertical orientations leads to a higher PCM temperature compared to the base case at the same time intervals. Furthermore, incorporating twisted tape into the pipe configuration has shown an additional elevation in the temperature of the PCM compared to the use of straight tape. Notably, the combination of helical fins with twisted tape configuration results in the highest PCM temperature among all cases at 5-min intervals. This observation suggests an enhanced heat transfer between the HTF and the PCM, leading to faster PCM melting due to the convection heat transfer caused by the rapid temperature rise, as shown in Fig. 5.

Fig. 11 illustrates the temperature distribution in the cross-sectional plane in the middle of the LHTES system at 10, 20, 30, and 40-min intervals. Each row corresponds to a different configuration, while the columns represent various time instances. The surface temperature distribution is presented using colour isolevels, with red denoting a temperature of 303.15 K and blue representing 358.15 K. The findings reveal that the configurations with fins and tapes result in higher PCM temperature compared to the base case at corresponding time intervals. Specifically, at shorter durations, at 10 and 20-min intervals, the helical fins configuration demonstrates a higher PCM temperature compared to both the horizontal fins and vertical fins configurations. However, during longer durations, such as 30 and 40 min, employing the vertical fins configuration yields a higher PCM temperature compared to both the helical and horizontal fins cases. Moreover, the incorporation of twisted tape yields higher PCM temperatures across all time durations when compared to configuration with straight tape. Additionally, the combination of helical fins with twisted tape consistently exhibits the highest PCM temperature among all cases at 10, 20, and 30-min intervals. Nonetheless, it is important to note that at 40-min intervals, the vertical fins case exhibits a slightly higher PCM temperature compared to the configuration with helical fins with twisted tape.

Fig. 12 shows the time evolution of the average PCM temperature for all configurations under the melting process within the LHTES system. The initial phase for all cases involves a gradual increase in the PCM temperature until it reaches its melting point, leading to the phase change from solid to liquid at almost constant temperature. Throughout this phase change, the PCM continues melting due to the convection heat transfer until all the PCM above the HTF tube is transformed into a liquid state (see Figs. 6 and 11). As heat is further added over time, the average PCM temperature continues to rise until it eventually reaches the HTF temperature of 358.13 K. Concurrently, heat is continuously transferred to the solid PCM located below the HTF tubes. The use of fins within the LHTES system facilitates a more rapid PCM melting process by enabling a swift temperature rise, as a result of higher convection currents. The addition of fins increases the external surface area, thereby enhancing heat transfer performance and ensuring efficient dissipation of heat from the pipe. Additionally, the fins help reduce temperature gradients within the PCM, resulting in a more uniform temperature distribution, preventing hotspots, and ensuring stable and predictable thermal performance compared to the base case, as depicted in Fig. 11. This effect of fins was also observed by Mahdi et al. [58] in shell and tube LHTES with five longitudinal fins and Mehta et al. [46] in shell and tube LHTES with helical fins. Conversely, the tape configurations act as a heat bridge across the HTF pipe, enhancing the heat transfer to the PCM by augmenting the internal wet surface area of the HTF pipe, as observed in configurations with tapes in Fig. 11. The configuration with helical fins and twisted tape provides a dual benefit, optimizing both the internal and external surface areas of the HTF tubes (Fig. 11). This combination leads to significant improvements in heat transfer from the HTF to the PCM. Over the time intervals ranging from 0 to 29 min, the

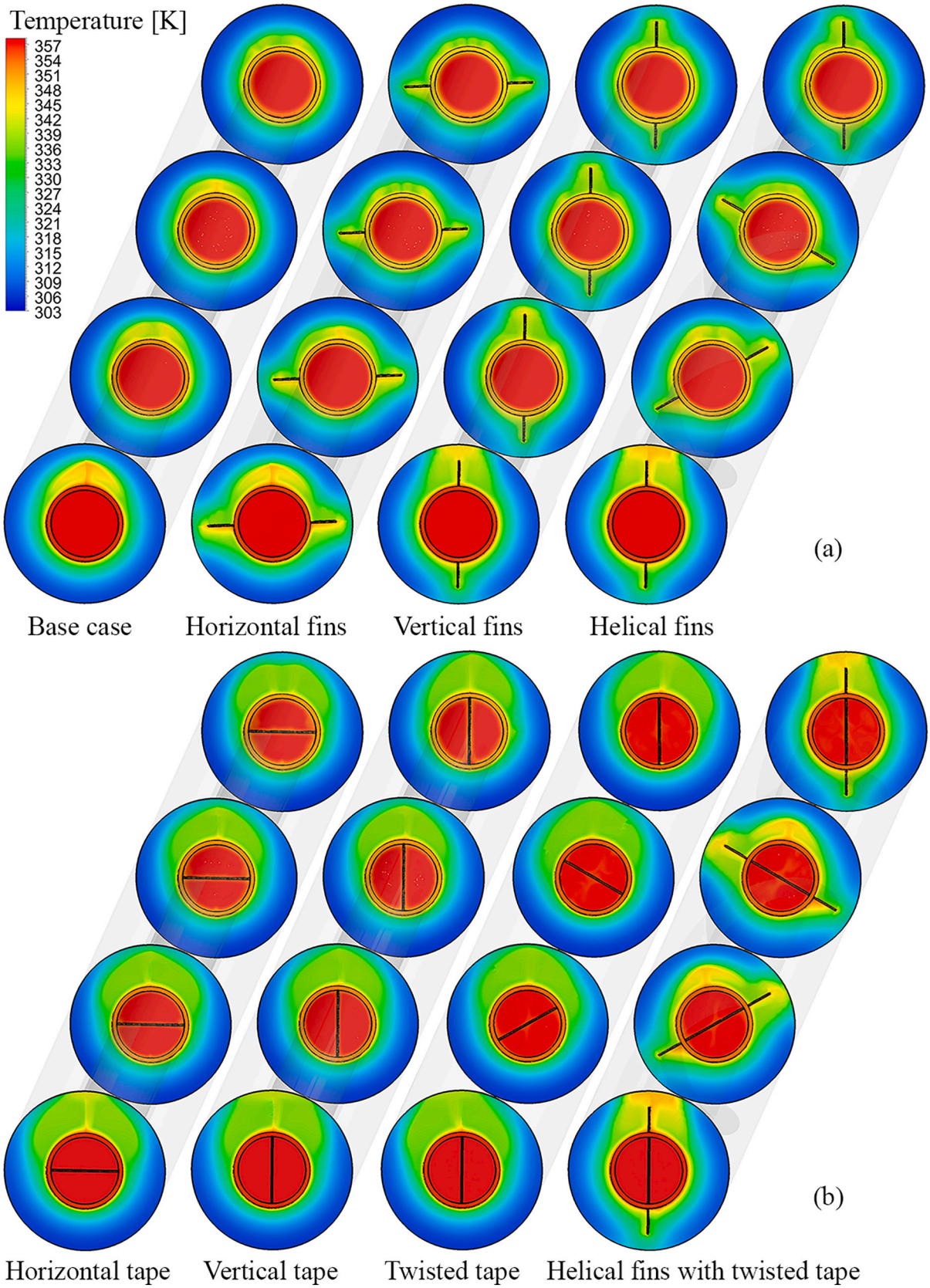

Fig. 10. Temperature distributions at four cross-sections in $x_1 = 0, 0.33$ m, 0.66 m and 1 m plane, including (a) the base case, horizontal fins, vertical fins, and helical fins and (b) horizontal tape, vertical tape, twisted tape, and combined helical fins with twisted tape, captured after 5 min from the start.

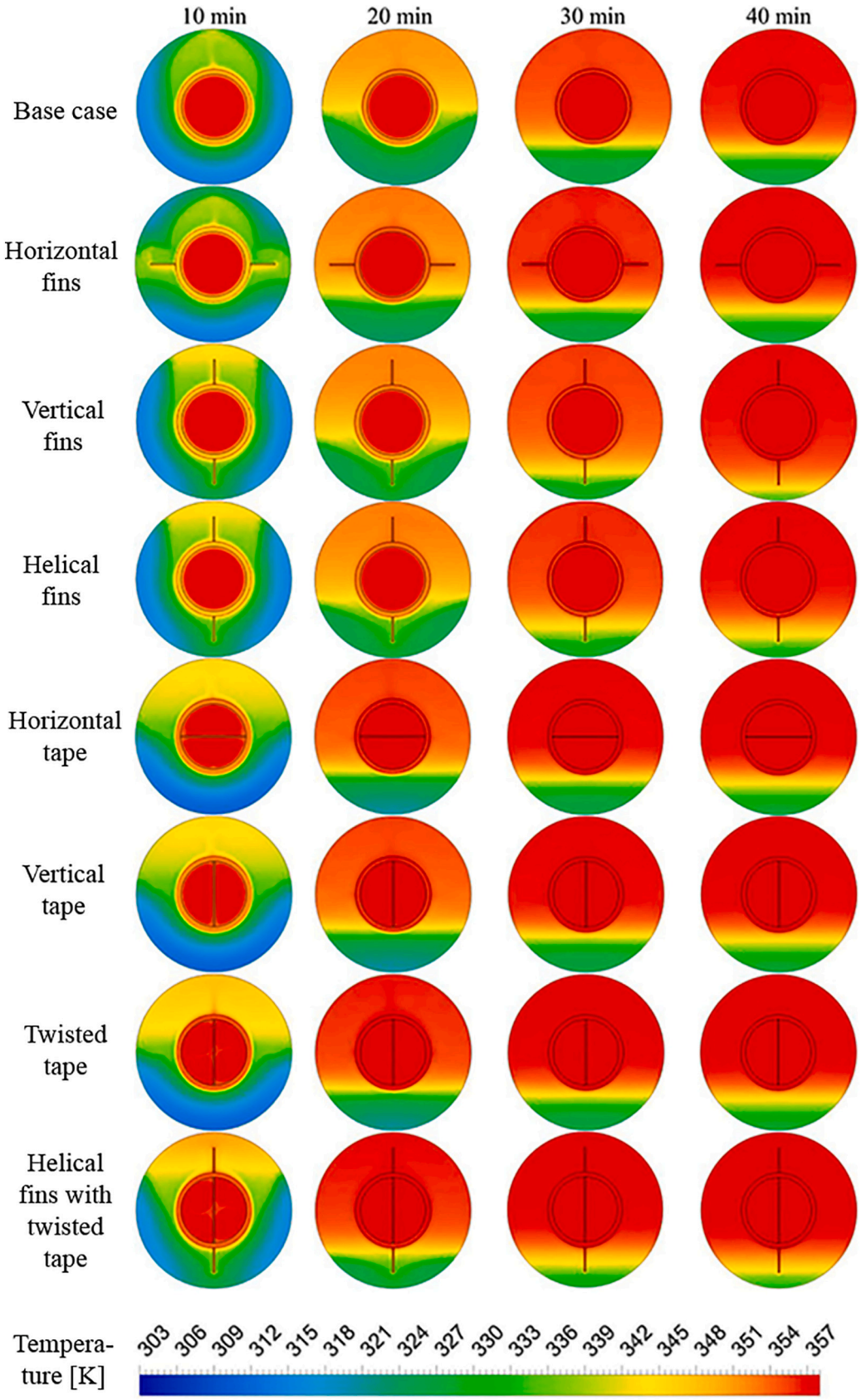

Fig. 11. Temperature distributions contours of the base case, horizontal fins, vertical fins, helical fins, horizontal tape, vertical tape, twisted tape, and combined helical fins with twisted tape are depicted using colour isolevels at 10, 20, 30, and 40-min intervals. These distributions are shown in the x_1 plane, specifically at a location 500 mm from the inlet.

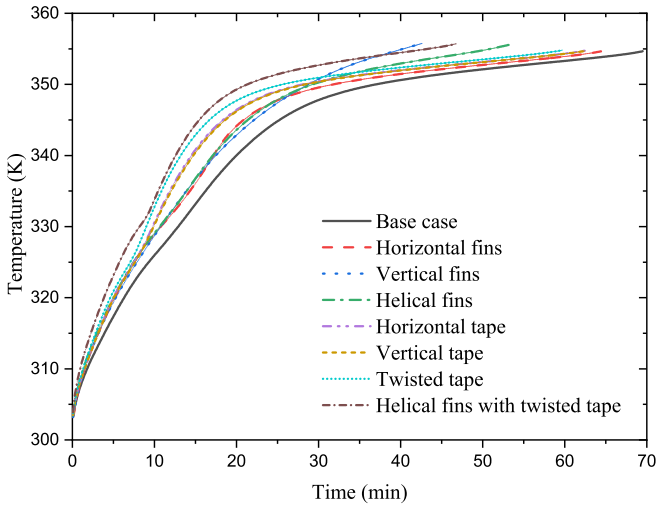

Fig. 12. PCM average temperature for the base case, horizontal fins, vertical fins, helical fins, horizontal tape, vertical tape, twisted tape, and combined helical fins with twisted tape, during the melting process.

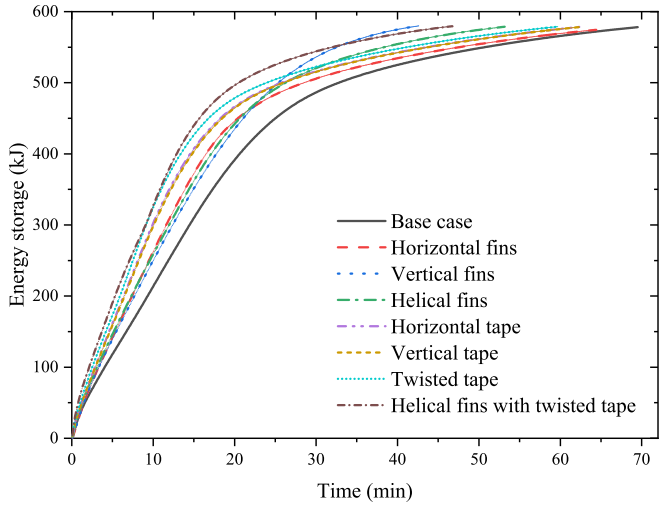

Fig. 13. The energy storage for the base case, horizontal fins, vertical fins, helical fins, horizontal tape, vertical tape, twisted tape, and combined helical fins with twisted tape, during the melting process.

configuration with combined helical fins with twisted tape consistently demonstrates the highest average PCM temperature among all the studied configurations. However, after 29 min, a slightly higher average PCM temperature is observed in the configuration with vertical fins compared to the combined configuration with helical fins and twisted tape. Furthermore, the results indicate that at certain time intervals, the use of both vertical fins and helical fins simultaneously leads to a notably higher average PCM temperature compared to the base case. Specifically, at intervals ranging from 0 to 22 min using the configuration with helical fins higher average PCM temperatures are observed compared to configurations with horizontal or vertical fins. However, for a prolonged duration, the configuration with vertical fins displays higher average PCM temperatures compared to both cases with helical and horizontal fins. The use of tape also contributes to an increase in the average PCM temperature, though to a lesser extent than using fins. The implementation of straight tape horizontally or vertically results in nearly similar average PCM temperatures, as they facilitate equivalent heat transfer to the PCM. Furthermore, both cases with horizontal and vertical tapes exhibit higher average PCM temperatures when compared to the equivalent base case. Nevertheless, the utilisation of twisted tape proves to be notably more effective, as it enables the attainment of even higher average PCM temperatures.

3.3. Effect of fins and tapes on the amount of stored energy

Fig. 13 illustrates the change of stored energy over time for different configurations during the melting phase within the LHTES system. The results of the investigation reveal noteworthy trends. Specifically, the introduction of fins and tapes causes a discernible shift of the curve to the left, indicating an accelerated rate of LHTES charging. Among all configurations, the configuration with helical fins exhibits better performance compared to the configurations with horizontal and vertical fins. However, over a longer time, the configuration with vertical fins demonstrates superior stored energy performance in comparison to both the configurations with helical and horizontal fins. While the implementation of tape contributes to an increase in average stored energy, its impact is relatively modest compared to the effect of fins. The use of straight tape in both horizontal and vertical orientations yields nearly equivalent average stored energy. Furthermore, the adoption of twisted tape appears as significantly more efficacious, enabling the attainment of even higher average stored energy levels. Similar trends have been observed in another study conducted by Modi et al. [57].

3.4. Effect of fins and tapes on the heat transfer rate and Nusselt number

In this study, the heat transfer rate and Nu numbers have been calculated to assess the thermal performance of the LHTES. Fig. 14(a) shows the variation of the average heat transfer rate over time for different configurations during the melting phase. At the beginning of the process, when the temperature difference between the PCM and the HTF is large, the heat transfer rate is the highest for all configurations. Due to the melting of the PCM around the HTF, the heat transfer rate decreases and becomes almost constant at a certain point, after about 40 min. The heat transfer rate for the base case is the lowest at the beginning of the process, but remains higher compared to the other configurations at the later stage of the PCM melting process. This implies that the use of fins and tape has a significant effect on the heat transfer rate at the beginning of the process, but their importance decreases at a later stage. Similar results of the variation of the heat transfer rate with time have been observed by Khan and Khan [54].

Fig. 14(b) shows the variation of the average Nusselt number with time for different configurations during the melting phase. *Nu* number gradually increases and then decreases during the process. The results show that the *Nu* number for the base case remains the highest compared to all other cases. A similar value of Nu number has been reported in other studies by Li et al. [25] and Shafiei Ghazani and Gholamzadeh [30].

3.5. Effect of twisted tape configuration on hydraulic characteristics

Fig. 15 presents a comparison of pressure drop (Δp) for different configurations at various Reynolds numbers. The configuration with the twisted tape exhibits the highest pressure drop among all tested configurations. The significant rise in pressure drop in the twisted tape configuration can be attributed to two primary factors. Firstly, the presence of the tape reduces the hydraulic diameter D_h resulting in higher flow resistance. Secondly, the twisting of the tape introduces additional blockage, further hindering the fluid flow. Notably, when comparing configurations at the same Reynolds number, the pressure drop difference between the setups with straight tape and those without tape is more pronounced than the contribution arising from the twisting of the tape. This indicates that the solid blockage caused by the presence of the tape has a more significant impact on the pressure drop compared to the effect of the tape twist. Despite the modest further increase in pressure drop observed in the twisted tape configuration, as illustrated in Fig. 15, the thermal performance benefits are considerable, as

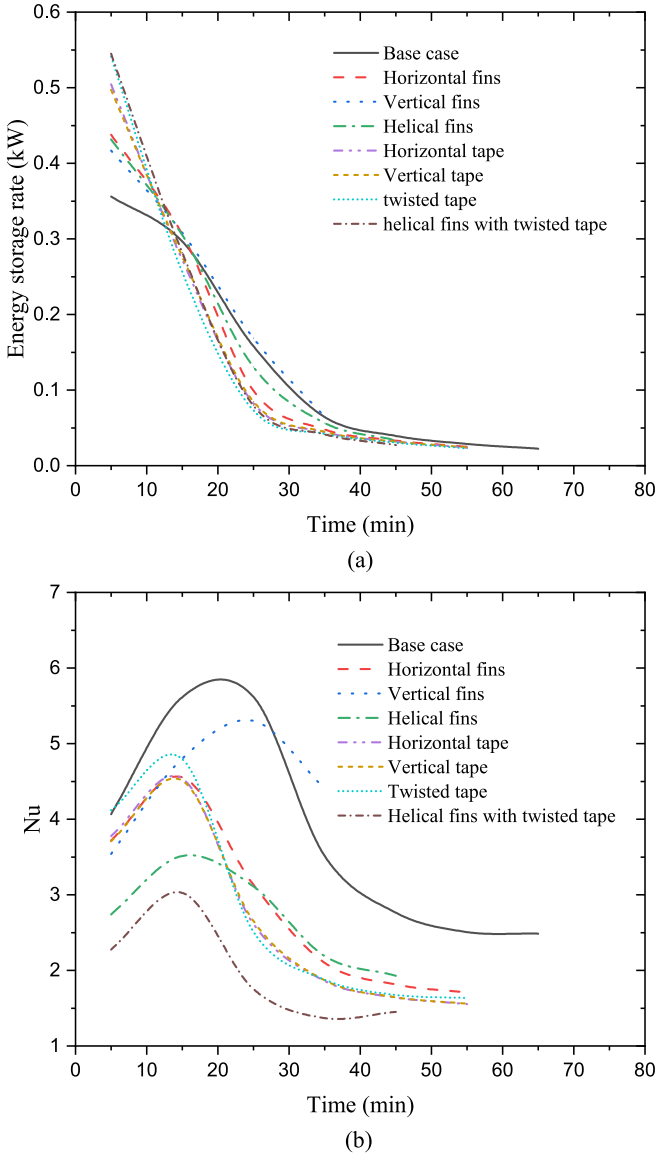

Fig. 14. The heat transfer rate (a) and *Nu* number (b) for the base case, horizontal fins, vertical fins, helical fins, horizontal tape, vertical tape, twisted tape, and combined helical fins with twisted tape, during the melting process.

demonstrated in Fig. 9. The incorporation of a tape twist leads to noteworthy gains in melting performance. Therefore, the pumping power needed for the configuration with twisted tape is only marginally higher than that needed for the straight tape setup. However, it is still significantly higher when compared to the LHTES without tape, at the same Reynolds number.

4. Conclusions

In this study, the influence of different pipe configurations with external fins and internal tapes on the melting process in a shell and tube Latent Heat Thermal Energy Storage (LHTES) system was investigated. Stearic acid served as the Phase Change Material (PCM), and water, heated to 358.13 K, as the Heat Transfer Fluid (HTF) was used. The configurations studied included: the base case with a simple pipe, a pipe with horizontal fins, a pipe with vertical fins, a pipe with helical fins, a pipe with horizontal internal tape, a pipe with internal vertical tape, a pipe with internal twisted tape, and pipe with helical fins with twisted tape.

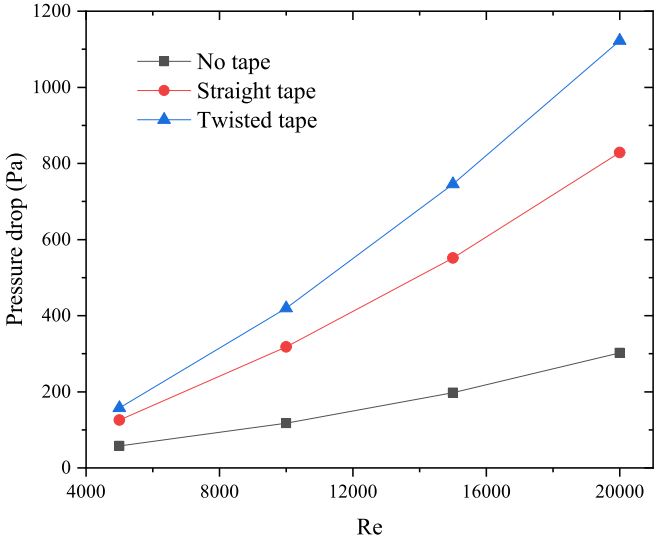

Fig. 15. The pressure drop Δp of LHTES, without a tape. Straight tape and twisted tape.

The use of horizontal fins, vertical fins, and helical fins leads to a significant enhancement in the melting process, reducing the full melting time by 7.2 %, 38.7 %, and 23.5 %, respectively, in comparison to the base case which was ~69 min where the simple straight pipe was used. By employing various configurations with external fins, the heat transfer surface area is increased, facilitating efficient heat transfer between the HTF tube and PCM. Simultaneously, this minimises temperature gradients within the PCM, leading to a more uniform temperature distribution and ensuring stable and predictable thermal performance.

The LHTES with tape also affects accelerated melting time, although to a lesser extent compared to fins. Specifically, twisted tape emerges as a highly effective promoter of enhanced heat convection due to the HTF's rotation about the LHTES axis. It is worth noting that the use of tape introduced a slight penalty in pressure drop, causing additional pumping power. Nevertheless, it still offers comparable thermal performance advantages compared to the base case.

The implementation of tapes in HTF pipes offers several practical advantages. Firstly, it helps increase heat transfer from the HTF pipe without impacting the PCM volume or its original shape. Secondly, the utilisation of tapes proves beneficial in scenarios where the installation of conventional fins on the HTF pipe is impractical or not feasible. In such cases, tapes provide a viable alternative for enhancing heat transfer within the system. Lastly, when combining helical fins with twisted tape, the resultant synergistic effect leads to the fastest melting rate. This innovative approach holds promise for achieving rapid and efficient phase change processes.

The melting performance is similar using both configurations with vertical and horizontal tapes, ensuring consistent heat transfer between the HTF and PCM. However, significant performance variations are observed using straight external vertical and horizontal fins. The vertical fins outperform horizontal fins in terms of rate of melting PCM, this is mainly because the lower fin in the vertical configuration is positioned closer to the lower part of the LHTES.

The combination of helical fins and twisted design led to the highest melting process within the range of 0 to 29 min. Then, the vertical fins design exhibits a slightly better melting process. This combination offers several practical benefits, providing rapid and efficient phase change transition without affecting the fluid flow pattern. Additionally, the fins or tapes inserted allow for further compaction of the LHTES designs, achieving a higher energy storage density and resulting in cost savings, especially when the PCM is expensive. This compact design leads to a lighter LHTES, making it fit for applications with limited space.

A detailed analysis of an HTF tube with fins and tape configurations shows that the use of helical fins and twisted tape configurations can significantly improve the thermal performance of LHTES. One of the problems associated with the use of these configurations is the difficulty in manufacturing this type of system. Therefore, the next phase of the study should focus on the optimisation of such LHTES systems taking into account the complexity of the manufacturing processes.

Also, the next important step in the development of LHTES is to develop mathematical models that allow researchers and engineers to predict the behaviour of different LHTES systems under different conditions and using different configurations and PCMs. By addressing these challenges, LHTES systems can play an important role in the development of sustainable thermal energy storage solutions.

The results of this study provide important guidelines for the design of thermal storage systems. It is expected that this study will significantly contribute to more efficient and economically practical LHTES systems for solar power plants, waste heat recovery systems, thermal energy storage systems, and heating and cooling systems.

CRediT authorship contribution statement

Abdullah Masoud Ali: Writing – original draft, Visualization, Validation, Software, Methodology, Investigation, Funding acquisition, Formal analysis, Data curation, Conceptualization. **Audrius Bagdanavicius:** Writing – review & editing, Supervision, Resources, Project administration, Methodology, Investigation, Funding acquisition. **Edward R. Barbour:** Writing – review & editing. **Daniel L. Pottie:** Writing – review & editing. **Seamus Garvey:** Writing – review & editing. **James Rouse:** Writing – review & editing. **Zahra Baniamerian:** Writing – review & editing.

Declaration of competing interest

The authors declare that they have no known competing financial interests or personal relationships that could have appeared to influence the work reported in this paper.

Data availability

No data was used for the research described in the article.

Acknowledgements

This research was supported by the UK EPSRC award “Sustainable, Affordable and Viable Compressed Air Energy Storage” (SAVE-CAES, EP/W027569/1). This research used the ALICE High Performance Computing Facility at the University of Leicester.

References

[1] P. Farzanehkhameneh, M. Soltani, F. Moradi Kashkooli, M. Ziabasharhagh, Optimization and energy-economic assessment of a geothermal heat pump system, Renew. Sust. Energ. Rev. 133 (2020) 110282.
[2] J.M. Mahdi, E.C. Nsofor, Multiple-segment metal foam application in the shell-and-tube PCM thermal energy storage system, J. Energy Storage 20 (2018) 529–541.
[3] A. Razmi, M. Soltani, M. Tayefeh, M. Torabi, M.B. Dusseault, Thermodynamic analysis of compressed air energy storage (CAES) hybridized with a multi-effect desalination (MED) system, Energy Convers. Manag. 199 (2019) 112047.
[4] S. Zhang, D. Feng, L. Shi, L. Wang, Y. Jin, L. Tian, Z. Li, G. Wang, L. Zhao, Y. Yan, A review of phase change heat transfer in shape-stabilized phase change materials (ss-PCMs) based on porous supports for thermal energy storage, Renew. Sust. Energ. Rev. 135 (2021) 110127.
[5] P.T. Sardari, R. Babaei-Mahani, D. Giddings, S. Yasseri, M.A. Moghimi, H. Bahai, Energy recovery from domestic radiators using a compact composite metal foam/PCM latent heat storage, J. Clean. Prod. 257 (2020) 120504.
[6] M. Javaheri, A. Shafiei Ghazani, Energy and exergy analysis of a novel advanced adiabatic compressed air energy storage hybridized with reverse osmosis system, J. Energy Storage 73 (2023) 109250.
[7] D.L. Pottie, M.M. Oliveira, B. Cardenas, Z. Baniamerian, S. Garvey, J. Rouse, E. Hough, A. Bagdanavicius, A.M. Ali, P. Eames, E.R. Barbour, Adiabatic compressed air energy storage system performance with application-oriented designed axial-flow compressor, Energy Convers. Manag. 304 (2024) 118233.
[8] A. Sciacovelli, F. Gagliardi, V. Verda, Maximization of performance of a PCM latent heat storage system with innovative fins, Appl. Energy 137 (2015) 707–715.
[9] S.-C. Costa, K. Mahkamov, M. Kenisarin, M. Ismail, E. Halimic, D. Mullen, K. Lynn, T. Werner, Experimental and numerical study on melting of solar salt in a finned metallic container, in: ASME 2018 International Mechanical Engineering Congress and Exposition, 2018.
[10] K. Bhagat, M. Prabhakar, S.K. Saha, Estimation of thermal performance and design optimization of finned multitube latent heat thermal energy storage, J. Energy Storage 19 (2018) 135–144.
[11] S.-C. Costa, K. Mahkamov, M. Kenisarin, M. Ismail, K. Lynn, E. Halimic, D. Mullen, Solar salt latent heat thermal storage for a small solar organic Rankine cycle plant, J. Energy Resour. Technol. 142 (3) (2019).
[12] M. Sheikholeslami, Numerical modeling of nano enhanced PCM solidification in an enclosure with metallic fin, J. Mol. Liq. 259 (2018) 424–438.
[13] A.N. Olimat, M. Ismail, N. Abu Shaban, A. Al-Salaymeh, The effectiveness of the heat transfer fluid pipe orientation angle inside a latent heat thermal energy storage system, Case Stud. Therm. Eng. 36 (2022) 102174.
[14] J.M. Mahdi, E.C. Nsofor, Solidification of a PCM with nanoparticles in triplex-tube thermal energy storage system, Appl. Therm. Eng. 108 (2016) 596–604.
[15] Y. Huo, Z. Rao, Lattice Boltzmann investigation on phase change of nanoparticle-enhanced phase change material in a cavity with separate plate, Energy Convers. Manag. 154 (2017) 420–429.
[16] E. Akyol, O. Hacıhafızoğlu, Ç. Susantez, K. Kahveci, U. Akyol, Experimental and numerical investigation of heat transfer in a channel with multiple phase change materials (PCMs), J. Energy Storage 45 (2022) 103710.
[17] L. Pu, S. Zhang, L. Xu, Z. Ma, X. Wang, Numerical study on the performance of shell-and-tube thermal energy storage using multiple PCMs and gradient copper foam, Renew. Energy 174 (2021) 573–589.
[18] J. Zhang, X. Zhang, Y. Wan, D. Mei, B. Zhang, Preparation and thermal energy proper- ties of paraffin/halloysite nanotube composite as form-stable phase change material, Sol. Energy 86 (5) (2012) 1142–1148.
[19] S. Pincemin, X. Py, R. Olives, M. Christ, O. Oettinger, Elaboration of conductive thermal storage composites made of phase change materials and graphite for solar plant, J. Solar Energy Eng. 130 (1) (2007).
[20] O. Mesalhy, K. Lafdi, A. Elgafy, K. Bowman, Numerical study for enhancing the thermal conductivity of phase change material (PCM) storage using high thermal conductivity porous matrix, Energy Convers. Manag. 46 (6) (2005) 847–867.
[21] A. Kumar, S.K. Saha, Energy and exergy analyses of medium temperature latent heat thermal storage with high porosity metal matrix, Appl. Therm. Eng. 109 (2016) 911–923.
[22] A. Felix Regin, S.C. Solanki, J.S. Saini, An analysis of a packed bed latent heat thermal energy storage system using PCM capsules: numerical investigation, Renew. Energy 34 (7) (2009) 1765–1773.
[23] W. Zhao, S. Neti, A. Oztekin, Heat transfer analysis of encapsulated phase change materials, Appl. Therm. Eng. 50 (1) (2013) 143–151.
[24] J. Duan, Y. Xiong, D. Yang, Study on the effect of multiple spiral fins for improved phase change process, Appl. Therm. Eng. 169 (2020) 114966.
[25] J. Li, Z.R. Abdulghani, M.N. Alghamdi, K. Sharma, H. Niyas, H. Moria, A. Arsalanloo, Effect of twisted fins on the melting performance of PCM in a latent heat thermal energy storage system in vertical and horizontal orientations: energy and exergy analysis, Appl. Therm. Eng. 219 (2023) 119489.
[26] M. Dadollahi, M. Mehrpooya, Modeling and investigation of high temperature phase change materials (PCM) in different storage tank configurations, J. Clean. Prod. 161 (2017) 831–839.
[27] A. Shahsavar, A. Shaham, P. Talebizadehsardari, Wavy channels triple-tube LHS unit with sinusoidal variable wavelength in charging/discharging mechanism, Int. Commun. Heat Mass Transf. 107 (2019) 93–105.
[28] R. Babaei, A. Shafiei Ghazani, Numerical investigation of melting process enhancement in shell and coil latent heat storage tanks by the simultaneous use of conical coil and conical shell, J. Energy Storage 86 (2024) 111173.
[29] Y. Zhao, Q. Mao, Experimental and numerical analysis of unsteady state conditions on thermal storage performance of a conical spiral shell-tube energy storage system, J. Energy Storage 88 (2024) 111579.
[30] A. Shafiei Ghazani, A. Gholamzadeh, The effect of conical shell and converging/diverging tube on the charging performance of shell and tube latent heat thermal energy storage system, J. Energy Storage 65 (2023) 107262.
[31] A.M. Abdulateef, S. Mat, J. Abdulateef, K. Sopian, A.A. Al-Abidi, Geometric and design parameters of fins employed for enhancing thermal energy storage systems: a review, Renew. Sust. Energ. Rev. 82 (2018) 1620–1635.
[32] M.K. Rathod, J. Banerjee, Thermal performance enhancement of shell and tube latent heat storage unit using longitudinal fins, Appl. Therm. Eng. 75 (2015) 1084–1092.
[33] E.G. Jung, J.H. Boo, Thermal analytical model of latent thermal storage with heat pipe heat exchanger for concentrated solar power, Sol. Energy 102 (2014) 318–332.
[34] A. Campos-Celador, G. Diarce, I. González-Pino, J.M. Sala, Development and compara- tive analysis of the modeling of an innovative finned-plate latent heat thermal energy storage system, Energy 58 (2013) 438–447.
[35] N.H.S. Tay, F. Bruno, M. Belusko, Comparison of pinned and finned tubes in a phase change thermal energy storage system using CFD, Appl. Energy 104 (2013) 79–86.
[36] A.A. Al-Abidi, S. Mat, K. Sopian, M.Y. Sulaiman, A.T. Mohammad, Numerical study of PCM solidification in a triplex tube heat exchanger with internal and external fins, Int. J. Heat Mass Transf. 61 (2013) 684–695.

[37] R. Baby, C. Balaji, Thermal optimization of PCM based pin fin heat sinks: an experimental study, Appl. Therm. Eng. 54 (1) (2013) 65–77.
[38] J.C. Choi, S.D. Kim, Heat-transfer characteristics of a latent heat storage system using MgCl2 · 6H2O, Energy 17 (12) (1992) 1153–1164.
[39] T. Alam, M.-H. Kim, A comprehensive review on single phase heat transfer enhancement techniques in heat exchanger applications, Renew. Sust. Energ. Rev. 81 (2018) 813–839.
[40] S. Ponnada, T. Subrahmanyam, S.V. Naidu, A comparative study on the thermal performance of water in a circular tube with twisted tapes, perforated twisted tapes and perforated twisted tapes with alternate axis, Int. J. Therm. Sci. 136 (2019) 530–538.
[41] A.M. Ali, A. Rona, H.T. Kadhim, M. Angelino, S. Gao, Thermo-hydraulic performance of a circular microchannel heat sink using swirl flow and nanofluid, Appl. Therm. Eng. 191 (2021).
[42] A.M. Ali, A. Rona, M. Angelino, Numerical investigation of various twisted tapes enhancing a circular microchannel heat sink performance, Int. J. Heat Fluid Flow 98 (2022) 109065.
[43] H. Arasteh, A. Rahbari, R. Mashayekhi, A. Keshmiri, R.B. Mahani, P. Talebizadehsardari, Effect of pitch distance of rotational twisted tape on the heat transfer and fluid flow characteristics, Int. J. Therm. Sci. 170 (2021) 106966.
[44] J.C. Kurnia, B.A. Chaedir, A.P. Sasmito, Laminar convective heat transfer in helical tube with twisted tape insert, Int. J. Heat Mass Transf. 150 (2020) 119309.
[45] H. Arjmandi, P. Amiri, M. Saffari Pour, Geometric optimization of a double pipe heat exchanger with combined vortex generator and twisted tape: a CFD and response surface methodology (RSM) study, Therm. Sci. Eng. Prog. 18 (2020) 100514.
[46] D.S. Mehta, B. Vaghela, M.K. Rathod, J. Banerjee, Heat transfer enhancement using spiral fins in different orientations of latent heat storage unit, Int. J. Therm. Sci. 169 (2021) 107060.
[47] S. Zhang, L. Pu, L. Xu, R. Liu, Y. Li, Melting performance analysis of phase change materials in different finned thermal energy storage, Appl. Therm. Eng. 176 (2020) 115425.
[48] A.D. Brent, V.R. Voller, K.J. Reid, Enthalpy-porosity technique for modeling convection-diffusion phase change: application to the melting of a pure metal, Numer. Heat Transf. 13 (3) (1988) 297–318.
[49] X.-L. Ouyang, R.-N. Xu, P.-X. Jiang, Three-equation local thermal non-equilibrium model for transient heat transfer in porous media: the internal thermal conduction effect in the solid phase, Int. J. Heat Mass Transf. 115 (2017) 1113–1124.
[50] Y. Wu, D. Li, W. Jiang, S. Zhu, X. Zhao, M. Arıcı, E. Tunçbilek, Energy storage and exergy efficiency analysis of a shell and tube latent thermal energy storage unit with non-uniform length and distributed fins, Sustain. Energy Technol. Assess. 53 (2022) 102362.
[51] ANSYS, 18.0 ANSYS Fluent Theory Guide 18.0, 2017.
[52] A.M. Ali, Analysis of the Heat Transfer and Flow in Minichannel and Microchannel Heat Sinks by Single and Two-phase Mixture Models, University of Leicester, 2023.
[53] A.M. Ali, M. Angelino, A. Rona, Numerical analysis on the thermal performance of microchannel heat sinks with Al_2O_3 nanofluid and various fins, Appl. Therm. Eng. 198 (2021) 117458.
[54] L.A. Khan, M.M. Khan, Role of orientation of fins in performance enhancement of a latent thermal energy storage unit, Appl. Therm. Eng. 175 (2020) 115408.
[55] R. Qaiser, M.M. Khan, L.A. Khan, M. Irfan, Melting performance enhancement of PCM based thermal energy storage system using multiple tubes and modified shell designs, J. Energy Storage 33 (2021) 102161.
[56] A.M. Ali, M. Angelino, A. Rona, Physically consistent implementation of the mixture model for modelling nanofluid conjugate heat transfer in minichannel heat sinks, Appl. Sci. 12 (14) (2022) 7011.
[57] N. Modi, X. Wang, M. Negnevitsky, Melting and solidification characteristics of a semi-rotational eccentric tube horizontal latent heat thermal energy storage, Appl. Therm. Eng. 214 (2022) 118812.
[58] M.S. Mahdi, A.F. Hasan, H.B. Mahood, A.N. Campbell, A.A. Khadom, A.M.e. A. Karim, A.O. Sharif, Numerical study and experimental validation of the effects of orientation and configuration on melting in a latent heat thermal storage unit, J. Energy Storage 23 (2019) 456–468.
[59] H. Soltani, M. Soltani, H. Karimi, J. Nathwani, Optimization of shell and tube thermal energy storage unit based on the effects of adding fins, nanoparticles and rotational mechanism, J. Clean. Prod. 331 (2022) 129922.
[60] M. Ismail, A.H. Alkhazaleh, J. Masri, A.M. Ali, M. Ali, Experimental and numerical analysis of paraffin waxes during solidification inside spherical capsules, Therm. Sci. Eng. Prog. 26 (2021) 101095.
[61] P.J. Roache, Verification and Validation in Computational Science and Engineering vol. 895, Hermosa, Albuquerque, NM, 1998.